Targeting mitophagy in *SRSF2* mutant hematologic malignancies

Xiaolei Liu[1], Sudhish A. Devadiga[1], Robert F. Stanley[2], Ryan Morrow[3], Kevin Janssen[3], Mathieu Quesnel-Vallières[4], Oz Pomp[5], Adam A. Moverley[5], Chenchen Li[1], Nicolas Skuli[1], Martin P. Carroll[1], Jian Huang[6], Douglas C. Wallace[3,7], Kristen W. Lynch[4], Omar Abdel-Wahab[2], Peter S. Klein[1,5,*]

1. Department of Medicine, Division of Hematology-Oncology, Perelman School of Medicine, University of Pennsylvania; Philadelphia, PA, USA.

2. Molecular Pharmacology Program, Sloan Kettering Institute, Memorial Sloan Kettering Cancer Center, New York, NY, USA.

3. Center for Mitochondrial and Epigenomic Medicine, Children's Hospital of Philadelphia, Philadelphia, PA 19104.

4. Department of Biochemistry and Biophysics, Perelman School of Medicine, University of Pennsylvania, Philadelphia, PA, USA.

5. Department of Cell and Developmental Biology, Institute for Regenerative Medicine, Perelman School of Medicine, University of Pennsylvania, Philadelphia, PA, USA.

6. Coriell Institute for Medical Research, Camden, NJ 08103.

7. Department of Pediatrics, Division of Human Genetics, Perelman School of Medicine, University of Pennsylvania, Philadelphia, PA 19104.

* Author for correspondence (lead contact), Email: pklein@pennmedicine.upenn.edu

Summary

Myelodysplastic syndrome (MDS) is a clonal disorder characterized by hyperproliferation and dysplasia of hematopoietic progenitor cells, deficiencies in circulating blood cells, and progression to acute myeloid leukemia (AML). Splicing factor mutations are common in MDS, but how they alter cellular functions remains unclear. We show that increased mitophagy is a common feature in *SRSF2*^{P95*} mutated MDS and AML. The *SRSF2*$^{P95H/+}$ mutation alters the splicing of multiple mRNAs encoding mitochondrial proteins, impairs mitochondrial function, and increases mitophagy compared to isogenic cells with wild-type *SRSF2*. We also identify a mechanism of mitochondrial surveillance mediated by *PINK1* (*PTEN Induced Kinase 1*). *PINK1* mRNA is alternatively spliced to a form that retains an intron with a premature termination codon, yielding an unstable mRNA and reduced *PINK1* mRNA abundance. Mitochondrial stress promotes excision of this poison intron, stabilizing the mRNA and increasing *PINK1* mRNA and protein. Similarly, *SRSF2*^{P95H} induces mitochondrial defects and increases *PINK1* expression by promoting removal of the poison intron. In contrast, disrupting splicing by inhibiting glycogen synthase kinase 3 promotes retention of the poison intron, reducing *PINK1* mRNA, impairing mitophagy, and activating apoptosis in *SRSF2*$^{P95H/+}$ cells. These data reveal a mechanism for sensing mitochondrial stress through *PINK1* splicing and identify increased mitophagy as both a hallmark and a therapeutic vulnerability in *SRSF2*^{P95H} mutant MDS and AML.

Keywords: myelodysplasia, splicing, serine and arginine rich splicing factor 2 (SRSF2), mitophagy, chronic myelomonocytic leukemia (CMML), acute myeloid leukemia (AML), glycogen synthase kinase-3 (GSK-3), PTEN-induced putative kinase (PINK1), autophagy, Parkinson's disease

Introduction

Myelodysplastic syndrome (MDS) is a clonal hematopoietic disorder characterized by hyperproliferative bone marrow, dysplastic hematopoietic cells, peripheral cytopenias, and high risk of progression to acute myeloid leukemia (AML). Recurrent mutations in RNA splicing factors (SFs), including *SF3B1*, *SRSF2, and U2AF1*, account for 60-70% of somatic mutations in MDS[1] and are common in myeloproliferative neoplasms (MPNs), the MDS/MPN overlap disorder chonic myelomonocytic leukemia (CMML), and AML[1-6]. However, the mechanisms by which these mutations alter cellular functions or contribute to transformation remain unclear.

Mutations in distinct SFs cause myeloid disorders with similar phenotypic features but limited overlap in specific mRNAs that are aberrantly spliced. This may suggest that distinct mRNA targets are responsible for these myeloid malignancies or that shared pathways are affected downstream of aberrantly spliced mRNAs. Hotspot mutations in *SRSF2* alter RNA binding site specificity and disrupt the splicing of mRNAs encoding hematopoietic regulators that are frequently mutated in AML[7,8]. For example, the *SRSF2*^{P95*} mutation promotes inclusion of a poison exon in *EZH2* mRNA, leading to nonsense mediated decay and reduced levels of *EZH2*[7]. Thus, the number of patients with reduced *EZH2* expression is significantly higher than the number with mutations in the *EZH2* gene per se[8]. These studies support a pathogenic mechanism targeting the splicing of a single mRNA, but do not rule out additional contributions from other splicing events. Furthermore, transcriptomic analyses of different SF mutants show that altered splicing of distinct mRNAs can affect common downstream pathways, including splicing itself, protein synthesis, and mitochondrial function[9].

Splicing factor mutations occur as mutually exclusive, heterozygous point mutations at specific residues[10,11]. The presence of a wild-type splicing factor is required for survival of MDS cells that express a mutant splicing factor, suggesting vulnerability associated with disrupted splicing factor activity. Consistent with this, hematopoietic cells with heterozygous splicing factor mutations are sensitized to additional perturbation of the splicing machinery by small molecule splicing inhibitors[12,13]. This observation has led to clinical trials with splicing inhibitors in refractory leukemia patients[12,14-18]. However, these trials have been ineffective so far[14], and there are currently no FDA-approved therapies that target splicing factors in MDS or AML.

Glycogen synthase kinase-3α/β (GSK-3α/β) are multifunctional serine/threonine kinases encoded by two similar genes, *GSK3A* and *GSK3B*. GSK-3 functions downstream of Flt3, c-Kit, and Wnt signaling, all pathways associated with MDS and AML[19]. *Gsk3a/b* double knockout (DKO) in mouse bone marrow causes a severe myeloproliferative phenotype with features similar to human MDS[20], but the substrates that mediate GSK-3 functions in mouse and human hematopoietic malignancies have not been extensively characterized. Our recent phosphoproteomic analysis of GSK-3 substrates identified multiple core splicing factors implicated in MDS and AML[19,21], consistent with prior studies supporting the importance of GSK-3 in splicing regulation[22-24]. Both pharmacological inhibition and genetic loss of *GSK3* disrupt pre-mRNA splicing on a transcriptome-wide scale in diverse cell types[19,25], raising the possibility that clinically well tolerated GSK-3 inhibitors could be repurposed to treat splicing factor mutant MDS and AML.

In the present study, we assessed transcriptome-wide changes in splicing upon GSK-3 inhibition (GSK-3i) in leukemic cells. We find that GSK-3i disrupts splicing and selectively kills MDS and AML cells with SF mutations. Mechanistically, GSK-3i induces a heightened splicing response in SF mutant cells by repressing cassette exon inclusion and promoting intron retention. *SRSF2* mutant cells show disrupted splicing of nuclear-encoded mitochondrial genes, impaired mitochondrial function, and an increase in mitophagy that is essential for their survival. Splicing of mRNA encoding the mitochondrial surveillance factor *PINK1* is altered in response to mitochondrial stress, leading to a more stable splice form and reflecting a novel mechanism for sensing mitochondrial stress. GSK-3i disrupts splicing of *PINK1*, promoting a splice form with a premature stop codon and reducing overall *PINK1* mRNA levels. The reduction in *PINK1* is associated with reduced mitophagy and enhanced apoptosis in splicing factor mutant cells, sparing cells with wild-type *SRSF2*. Our findings reveal a novel mechanism for mitochondrial surveillance and identify a new therapeutic vulnerability in splicing factor mutant MDS and AML.

Results

Preferential sensitivity of spliceosomal mutant leukemia to GSK-3i

Heterozygous splicing factor mutations sensitize leukemic cells to additional perturbation of the core splicing machinery[13]. As GSK-3 regulates splicing of a broad range of mRNAs in other cell types[21,25], we tested whether GSK-3i would enhance cell death in leukemic cells with heterozygous knockins of recurrent driver mutations in *SRSF2* and *SF3B1*. Isogenic *SRSF2*$^{P95H/+}$ and *SF3B1*$^{K700E/+}$ knock-in K562 cells[13] were cultured with the GSK-3 inhibitor CHIR99021 (CHIR) or vehicle control and proliferation was monitored at 2 and 4 days. Both *SRSF2*$^{P95H/+}$ and *SF3B1*$^{K700E/+}$ cells were preferentially sensitive to CHIR (Fig. 1a and Supplemental Fig. 1a) and the clinically well tolerated GSK-3 inhibitor lithium (Supplemental Fig.1b) compared to isogenic cells with wild-type (*WT*) *SRSF2* and *SF3B1*. A flow cytometric assay for apoptosis revealed that GSK-3i promotes both early and late apoptosis (Fig. 1b) in splicing factor mutant cells compared to parental cells but had little impact on their cell cycle status (Supplemental Fig. 1c). GSK-3i significantly activated extrinsic apoptosis, as indicated by increased cleaved caspase 8 in splicing factor mutant cells upon CHIR treatment (Fig. 1c). Moreover, the apoptosis induced by CHIR in *SF3B1*$^{K700E/+}$ was completely rescued by the caspase 8 specific inhibitor ZIETD and pan-caspase inhibitor ZVAD (Fig. 1d). Collectively, these data demonstrate that GSK-3i preferentially kills spliceosomal mutant leukemias by activating extrinsic apoptosis.

As an alternative approach to compare the effect of mutated and wild-type *SRSF2* in otherwise genetically identical cells, we introduced *SRSF2*^{P95H} or *SRSF2*^{wt} into parental TF-1 or K562 cells along with mCherry (Supplemental Fig. 1d, e), and then followed proliferation of mCherry positive and untransduced cells. Expression of *SRSF2*^{P95H} resulted in a competitive disadvantage when compared with the WT-expressing cells (Supplemental Fig. 1f), consistent with prior reports[7,26]. Further, GSK-3i markedly increased apoptosis in TF-1 and K562 cells expressing *SRSF2*^{P95H} compared to parental cells and cells overexpressing *SRSF2*^{wt} (Fig. 1e and Supplemental Fig. 1g). Therefore *SRSF2*^{P95H} confers sensitivity to GSK-3i whether introduced as a heterozygous knockin or overexpressed in a genetically identical background.

We next tested whether GSK-3i selectively kills splicing factor mutant cells *in vivo* in NSG mice bearing xenografts of isogenic *WT* and *SRSF2*$^{P95H/+}$ K562 cells (Fig. 1f). Daily administration of CHIR slowed the growth of xenografts with *SRSF2*$^{P95H/+}$ (p=0.0036), but had no significant effect on *SRSF2*^{wt} xenografts (Fig. 1g and supplemental Fig. 1h, i).

GSK-3i induces cell death in splicing factor mutant cells from patients with hematologic malignancies

Based on the promising results with leukemic cell lines (Fig. 1), we evaluated the preferential cytotoxicity of GSK-3i in primary cells from patients with AML or the MDS/MPN overlap disorder CMML. GSK-3i induced apoptosis in primary cells from patients with CMML or AML with *SRSF2*, *SF3B1*, or *U2AF1* mutations, but not in leukemic cells with wild-type splicing factors or in CD34^{+} cells from healthy subjects (Fig. 2a, and Supplemental Table 1).

Given the heterogeneity of primary human AML cells, we also tested the preferential cytotoxicity of GSK-3i in an isogenic context by expressing *SRSF2*^{WT} or *SRSF2*^{P95H} with mCherry in primary blasts from AML patients with wild-type splicing factors and then assessing the loss of mCherry positive cells over time with or without CHIR treatment (Fig. 2b). Primary AML cells expressing *SRSF2*^{P95H} were preferentially depleted upon CHIR exposure (Fig. 2c). In contrast, GSK-3i had no substantial effect on primary AML cells expressing *WT SRSF2* (Fig. 2c). Cells expressing mutant *SRSF2* also displayed a higher level of apoptosis in response to CHIR treatment relative to controls transduced with wild-type *SRSF2* (Fig. 2d). These data show that *SRSF2*^{P95H} confers sensitivity to GSK-3i.

GSK-3i alters global gene expression and splicing in human leukemic cells

To understand the functional consequences of GSK-3i on gene expression and splicing, we performed deep RNA-sequencing (RNA-seq) of parental K562 and isogenic *SRSF2*$^{P95H/+}$ and *SF3B1*$^{K700E/+}$ lines treated with or without CHIR (Fig. 3a and Supplemental Fig. 3a). CHIR treatment had distinct effects on the transcriptomes of WT, *SRSF2*$^{P95H/+}$, and *SF3B1*$^{K700E/+}$ mutant cells (Supplemental Fig. 3b, c, and supplemental table 2). Additionally, GSK-3i altered the expression of multiple *BCL2* family genes in a manner that promotes apoptosis (Supplemental Fig. 3d), consistent with the elevated apoptosis shown in Figure 1. CHIR treatment decreased abundance of mRNA encoding the anti-apoptotic *BCL-XL* (*BCL2L1*-encoded) and increased the pro-apoptotic genes *BAK1*, *BCL2L11*, and *BIK* regardless of SF mutation status. Previous work has suggested that splicing targeted therapies induce apoptosis through alternative splicing of *BCL2* family genes[27-29] and the combination of BCL-XL inhibition and SF3b-targeting splicing modulators enhances cytotoxicity in cancer cells[29]. To investigate whether BCL-XL inhibition mimics GSK-3i in SF mutant cells, we tested combinatorial effects of splicing factor mutation and BCL-XL inhibition. BCL-XL inhibition with A1155463 resulted in a higher level of apoptosis in SF mutant cells compared to parental controls (Supplemental Fig. 3e), suggesting that the reduced expression of *BCL-XL* upon CHIR exposure may contribute to the preferential sensitivity of SF mutant cells to GSK-3i. *BCL-X* is frequently regulated by alternative splicing, switching between the anti-apoptotic splice form (BCL-XL) to pro-apoptotic form (BCL-XS)[27-29]. However, the fraction of *BCL-XS* is unchanged upon CHIR treatment of cells with wild-type or mutant SFs (Supplemental Fig. 3f).

We then performed genome-wide analysis of splicing using the rMATS pipeline[30]. We measured the change in percentage spliced in (dPSI) values across five main types of alternative splicing (AS) events (skipped exon [SE], alternative 5' splice-site exon [A5SS], alternative 3' ss exon [A3SS], mutually exclusive exons [MXE], and retained introns [RI]) in CHIR-treated versus control (Supplemental table 3). Using a false discovery rate (FDR) of < 0.05 and dPSI >10% (Fig. 3b), we identified 549 alternatively spliced mRNAs in parental cells, 558 in *SRSF2*$^{P95H/+}$ and 694 in *SF3B1*$^{K700E/+}$ cells. However, only a relatively small fraction of the differentially spliced mRNAs were found in all the three genotypes upon GSK-3i, suggesting that GSK-3i has distinct and independent consequences on splicing in *WT* and splicing factor mutant cells (Fig. 3c and Supplemental Fig. 3g). The predominant change in RNA splicing upon CHIR treatment in *SRSF2*$^{P95H/+}$ and *SF3B1*$^{K700E/+}$ cells was increased cassette exon skipping relative to DMSO-treat controls, while approximately equal proportions of exon inclusion and exclusion with CHIR exposure were observed in parental cells (Fig. 3d). SF3B1 normally facilitates 3′ splice site recognition and is involved in the splicing of most introns by binding to the branchpoint[31]. GSK-3i in *SF3B1*$^{K700E/+}$ cells resulted in a higher proportion of repressed A3'SS (Fig. 3e) and increased number of RI events (Fig. 3b). Consistent with the distinct effects of GSK-3i on splicing in cells with *WT* vs mutant SFs, multiple regulators of hematopoietic cell survival and proliferation were alternatively spliced only in SF mutant K562 cells (Fig. 3f and Supplemental Fig. 3h). Among them, GSK-3i enhanced exon skipping in *DEPDC1* pre-mRNA in *SRSF2*$^{P95H/+}$ cells compared to wild-type counterparts, an event that was further validated by transcript specific RT-qPCR (Fig. 3f). Taken together, inhibition of GSK-3 further reduces splicing fidelity in splicing factor mutant hematopoietic cells, likely explaining the selective toxicity of GSK-3i to splicing factor mutant leukemias over wild-type counterparts.

GSK-3 regulates *PINK1* splicing

To test whether genes that are alternatively spliced following GSK-3i contribute to the preferential killing of spliceosome-mutant cells, we evaluated transcripts that exhibit concomitant dysregulation in gene expression and splicing with CHIR treatment (Fig. 4a). We focused our attention initially on *PINK1* because it is a serine/threonine kinase that serves as a critical sensor of mitochondrial damage and activates mitophagy to maintain mitochondrial homeostasis[32]. GSK-3i reduces the abundance and alters the splicing of *PINK1* mRNA in *WT*, *SRSF2*$^{P95H/+}$, and *SF3B1*$^{K700E/+}$ K562 cells. A Sashimi plot shows that GSK-3i enhances the retention of intron-6, which includes a premature termination codon (PTC) that is predicted to promote mRNA degradation through nonsense mediated decay (NMD) (Fig. 4b). RT-qPCR confirms that the abundance of *PINK1* is reduced in *WT*, *SRSF2*$^{P95H/+}$, and *SF3B1*$^{K700E/+}$ cells (Fig. 4c). This change in *PINK1* abundance was not due to a change in transcription, as detection of primary transcripts with PCR primers that detect intron-1 or intron-5 showed no significant difference in nascent transcripts with GSK-3i in *WT* or splicing factor mutant cells (Fig. 4d). Qualitative RT-PCR with primers that span exons 6 and 7 confirmed that CHIR impaired excision of intron-6, increasing intron-6 retention (568bp), in *SRSF2*$^{+/+}$, *SRSF2*$^{P95H/+}$, and *SF3B1*$^{K700E/+}$ K562 cells (Fig. 4e). CHIR also promoted retention of intron-6 in primary cells from patients with AML and CD34^{+} cells from healthy donors and CMML patients (Fig. 4f). To confirm that CHIR impairs *PINK1* splicing through inhibition of GSK-3, we tested *PINK1* splicing in *WT* and *GSK3A/B* DKO cells. Similar to CHIR, *GSK3A/B* DKO impaired intron-6 excision. In contrast, overexpression of *GSK3B* in DKO cells restored excision of intron-6 (Fig. 4g). Taken together, these data show that GSK-3 regulates PINK1 splicing and that CHIR

reduces *PINK1* mRNA abundance specifically by inhibiting GSK-3 and promoting retention of an intron containing an in-frame PTC.

SRSF2^{P95H} increases *PINK1* expression and mitophagy

In contrast to GSK-3i, the *SRSF2*^{P95H} mutation markedly increases *PINK1* mRNA abundance compared to parental and *SF3B1*$^{K700E/+}$ cells (Fig. 4c). Nascent *PINK1* transcripts were not increased in *SRSF2*$^{P95H/+}$ cells (Fig 4d), indicating that the increase in mRNA abundance was due to stabilization of the *PINK1* transcript rather than increased transcription. In support of this, excision of intron-6 was increased in *SRSF2*$^{P95H/+}$ cells compared to parental cells or *SF3B1*$^{K700E/+}$ cells (Fig 4e). Increased excision of intron-6 was further validated in TF-1 cells overexpressing *SRSF2*^{P95H} compared to cells expressing *SRSF2*^{wt} (Supplemental Fig. 5a). PINK1 activates mitophagy, and in parallel with the increase in *PINK1* levels, expression of other mitophagy-related genes, including *OPTN*, *ULK1*,*TOMM7*, *CALCOCO2*, *NBR1*, and *TAX1BP1,* was significantly increased in *SRSF2*$^{P95H/+}$ cells (Fig. 5a). The increase in *PINK1* and other mitophagy markers was associated with a substantial increase in mitophagy specifically in *SRSF2*$^{P95H/+}$ cells, as determined by the colocalization of TOMM20 (mitochondrial marker) and LAMP1 (lysosomal marker) (Fig. 5b). Transmission electron microscopy (TEM) showed accumulation of autophagic vacuoles with defective mitochondria with swollen matrix and collapsed cristae enclosed by a double membrane (Fig. 5c). As *SRSF2*^{P95H} and GSK-3i appear to have opposing effects on *PINK1* splicing and abundance, we tested the effect of CHIR on mitophagy in *SRSF2*$^{P95H/+}$ cells and found that GSK-3i impairs mitophagy in *SRSF2*$^{P95H/+}$ cells (Fig. 5b and 5c), in parallel with the reduction in *PINK1* mRNA. Consistent with elevated mitophagy in *SRSF2*$^{P95H/+}$ cells, western blot analysis confirmed that PINK1 protein is increased in *SRSF2*$^{P95H/+}$ cells but decreased upon CHIR treatment (Fig. 5d).

To address whether an increase in mitophagy is a feature of primary cells from patients with hematological malignancies, we queried the Cancer Genome Atlas database for expression of markers of mitophagy in hematologic malignancies with or without the *SRSF2* mutation. Expression of the canonical mitophagy markers *OPTN* ($p = 0.0015$), *ULK1* ($p = 0.0008$) and *TOMM7* ($p = 0.0004$) was significantly increased in patients with *SRSF2*^{P95*} (n = 43) compared to patients with wild-type *SRSF2* (n = 538) (Fig. 5e). No significant difference was observed between patients with *WT* and mutant *SF3B1* (Supplemental Fig. 5b). High *OPTN* expression is also associated with lower overall survival among AML patients in the TCGA dataset (Fig. 5f), consistent with reports showing lower survival in AML patients with elevated expression of autophagy markers[33] and MDS, MPN, and AML patients with *SRSF2* mutations[34-37]. These data show that elevated mitophagy marker expression is a common feature in *SRSF2* mutant MDS and AML and predicts a poor prognosis.

The *SRSF2* mutation is associated with accumulation of defective mitochondria

This increase in mitophagy indicates that the *SRSF2*$^{P95H/+}$ mutation causes mitochondrial dysfunction, which could arise through mis-splicing of nuclear mRNAs encoding mitochondrial proteins. We analysed splicing variations in *SRSF2*$^{P95H/+}$ cells compared to *SRSF2*$^{+/+}$ cells (Supplemental Fig. 6a). Gene ontology (GO) analysis of differentially spliced genes in *SRSF2*$^{P95H/+}$ cells revealed enrichment of processes related to regulation of protein targeting to mitochondrion organization, mitochondrial

genome maintenance, mitochondrial respiratory chain complex I assembly, and oxidative phosphorylation (Fig. 6a). We identified 12 alternatively spliced mRNAs that are associated with mitochondrial respiratory chain complex I (Fig. 6a). These findings are consistent with GO analyses in *SRSF2* mutant cells from primary MDS[9], CMML (Fig. 6b)[7], and AML patients (Fig. 6b)[7,38], which similarly showed enrichment of mitochondrial genes in the set of alternatively spliced mRNAs.

To further assess the consequences of *SRSF2* mutation on the cellular proteome in myeloid neoplasms, we performed quantitative mass spectrometry (qMS) with a focus on the mitochondrial proteome by using human proteome (UniprotKB) and mitochondrial (MitoCarta 3.0) databases for protein identification (Fig. 6c). We identified 163 mitochondrial proteins whose levels are affected by *SRSF2* mutation (Supplemental Table 4). The 84 proteins that showed significantly reduced levels in *SRSF2*$^{P95H/+}$ cells included multiple mitochondrial ribosomal proteins (Fig. 6d). Of the 6 respiratory mitochondrial complex 1 proteins detected by qMS, 5 were significantly downregulated by *SRSF2* mutation (Fig. 6d).

Evaluation of the mitochondrial properties of *SRSF2*$^{P95H/+}$ cells revealed elevated mitochondrial mass compared to *SRSF2*$^{+/+}$ cells based on mito-tracker green (MTG) staining (Fig. 6e) and immunostaining of the outer membrane protein TOMM20 (Supplemental Fig. 6b). Overexpression of *SRSF2*^{P95H} also increased mitochondrial content in K562, TF-1, and primary AML cells when compared with the overexpression of *WT SRSF2* (Supplemental Fig. 6c-e). Mitochondrial DNA (mtDNA) copy number, which correlates with mitochondrial biogenesis, significantly increased (Fig. 6f), suggesting that elevated mitophagy in *SRSF2*^{P95H} cells is balanced by increased mitochondrial biogenesis. This dynamic ultimately leads to increased mitochondrial content. Mitochondrial membrane potential (MMP) per unit mitochondrial mass as assessed by tetramethylrhodamine ethyl ester (TMRE)/MTG ratio was significantly higher in *SRSF2*$^{P95H/+}$ cells (Fig. 6g). To test mitochondrial function, we subjected parental and *SRSF2*$^{P95H/+}$ cells to high resolution respirometry. Surprisingly, both the basal and maximal respiratory capacity were significantly lower in *SRSF2*$^{P95H/+}$ cells (Fig. 6h). As *SRSF2* mutation dramatically altered the splicing of complex I related genes and reduced complex I protein levels, we further tested complex I respiratory capacity. Complex I-linked respiration, which was measured by sequential addition of the complex I-linked substrates pyruvate, malate, and glutamate (P/M/G) and ADP, was also significantly lower in *SRSF2*$^{P95H/+}$ cells relative to *SRSF2*$^{+/+}$ cells (Fig. 6h). The elevated mitochondrial mass and MMP in *SRSF2*$^{P95H/+}$ cells therefore could not maintain high respiratory capacity. These functional data together with the increase in mitophagy demonstrate a marked defect in mitochondrial function associated with the leukemogenic *SRSF2*^{P95H} mutation.

We next treated *WT* and *SRSF2*$^{P95H/+}$ K562 cells with a mitochondrial uncoupler, carbonyl cyanide m-chlorophenylhydrazone (CCCP) and then measured mitochondrial depolarization occurring during apoptosis using JC-1 staining[39]. Although *WT* cells responded to CCCP treatment with reduced MMP, the *SRSF2* mutation further decreased MMP, suggesting a higher demand for efficient mitophagy in response to mitochondrial stress in *SRSF2*$^{P95H/+}$ cells (Fig. 6i). Overall, these data support a model in which splicing defects associated with the *SRSF2* mutation disrupt mitochondrial function and lead to compensatory increased mitochondrial content and turnover.

As *SRSF2*^{P95H} increases the abundance of *PINK1* mRNA, we further hypothesize that mitochondrial dysfunction signals to the splicing apparatus to promote excision of intron-6, stabilizing *PINK1* mRNA to meet an increased demand for mitophagy. In support of this hypothesis, addition of CCCP promotes excision of intron-6 in a dose-dependent manner in cells with wild-type *SRSF2* and to an even greater extent in *SRSF2*$^{P95H/+}$ cells (Fig. 6j). Consistent with the destabilizing impact of the PTC in intron-6, this shift in splicing was associated with an increase in *PINK1* mRNA abundance (Fig. 6k). This response in cells with wild-type *SRSF2* as well as *SRSF2*$^{P95H/+}$ cells suggests a general mechanism, independent of the *SRSF2* mutation, for sensing mitochondrial stress through modulation of *PINK1* splicing, leading to increased *PINK1* expression and increased mitophagy.

Increased mitophagy is a therapeutic vulnerability in *SRSF2* mutant hematologic malignancies

GSK-3i reduces *PINK1* expression, impairs mitophagy, and is selectively lethal to *SRSF2*$^{P95H/+}$ cells. Given that PINK1-mediated mitophagy is required for the survival of normal hematopoietic stem cells (HSCs)[40] and acute myeloid leukemia stem cells (LSCs)[41,42], we hypothesized that a greater dependency on PINK1-mediated mitophagy upon stress may be the basis for the selective toxicity of GSK-3i to *SRSF2*$^{P95H/+}$ cells. To explore this hypothesis, we evaluated the effects of GSK-3i on mitochondria. GSK-3i with CHIR increased MMP (Fig. 7a) and promoted accumulation of mitochondrial mass in K562 cells with *WT SRSF2* (Fig. 7b), consistent with previous reports in mouse cardiomyocytes and HSCs[43,44]. GSK-3i in *SRSF2*$^{P95H/+}$ cells impaired mitophagy (Fig. 5b and 5c) and further increased MMP (Fig. 7a) and mitochondrial content (Fig. 7b and supplemental Fig. 7a, b, c) compared to *WT* counterparts. Gene set enrichment analysis (GSEA) revealed that GSK-3i with CHIR strongly enriches for genes representing enhanced mitochondrial biogenesis and oxidative phosphorylation (OXPHOS), a mitochondrial stress that may increase the requirement for PINK1-mediated mitochondrial surveillance (Fig. 7c).

To test directly whether GSK-3i-induced alternative splicing of *PINK1* causes cell death in *SRSF2*$^{P95H/+}$ cells, we expressed a *PINK1* cDNA lacking intron-6 and treated with CHIR (Fig. 7d). Expression of full length *PINK1* completely rescued the cell death caused by GSK-3i in *SRSF2*$^{P95H/+}$ cells (Fig. 7e), demonstrating an essential role for *PINK1* mis-splicing in the preferential cytotoxicity of GSK-3i in *SRSF2* mutant cells. These data support the hypothesis that aberrant splicing of *PINK1* caused by GSK-3i reduces *PINK1* expression and inhibits clearance of defective mitochondria in *SRSF2* mutant cells, disrupting the homeostatic balance required for survival (Fig. 7f).

Our data indicate that increased mitophagy is a targetable vulnerability in *SRSF2*$^{P95H/+}$ cells. We tested this hypothesis further by inhibiting mitophagy downstream of PINK1 by treating *SRSF2*$^{+/+}$ and *SRSF2*$^{P95H/+}$ cells with chloroquine (CQ), which blocks autophagic flux and mitophagy by inhibiting lysosomal acidification. Inhibiting mitophagy with CQ caused accumulation of mitochondria (Fig. 7g) and preferentially killed *SRSF2*$^{P95H/+}$ cells (IC_{50} = 14.1μM) compared to *SRSF2*$^{+/+}$ cells (IC_{50} = 29.1μM) (Fig. 7h, and supplemental Fig. 7d). Next, we introduced *SRSF2*^{P95H} or *SRSF2*^{wt} into *SRSF2*$^{+/+}$ primary AML cells along with the mCherry reporter (Fig. 7i). Expression of *SRSF2*^{P95H} resulted in increased sensitivity to CQ compared to WT-expressing primary AML cells (Fig. 7j). These data show that targeting mitophagy represents a promising therapeutic strategy to eradicate *SRSF2* mutant hematologic malignancies (Fig. 7f).

Discussion

Splicing factor mutations are common in MDS and AML[2,45,46], but how these mutations alter cellular function remains unclear. The results presented here show that increased mitophagy is a hallmark of *SRSF2* mutant MDS and AML. The recurrent *SRSF2*^{P95H} mutation alters the splicing of mRNAs encoding mitochondrial proteins, disrupts mitochondrial function, and increases mitochondrial mass and turnover, reflecting a dependency on a higher level of mitophagy for survival. Our results identify a mechanism of mitochondrial surveillance in which mitochondrial dysfunction enhances the splicing of *PINK1* mRNA to a more stable form, leading to increased abundance of *PINK1* mRNA and protein. Inhibition of GSK-3 impairs *PINK1* splicing, reduces mitophagy, and selectively kills cells with the *SRSF2*^{P95H} mutation. Inhibition of mitophagy by targeting lysosomal function is also lethal to *SRSF2*$^{P95H/+}$ cells. These data therefore reveal a novel dependency of splicing factor mutant MDS and AML and identify potential new therapeutic targets for these hematologic malignancies.

The altered splicing of nuclear encoded mitochondrial mRNAs observed here fits well with previous work identifying altered splicing of mRNAs involved in mitochondrial function in primary cells from MDS and AML patients with the *SRSF2*^{P95} mutation[7,9,38]. We also find that markers of mitophagy are robustly increased in AML and MDS patients in the TCGA dataset. Mitochondrial turnover is required for self-renewal of normal HSCs[40,47] and leukemic stem cells[42,48], and was recently shown to mediate resistance to BH3 mimetics in AML cells[33]. However, a critical dependence on increased mitophagy has not previously been described as a consequence of pathogenic splicing factor mutations.

The data presented here reveal a novel homeostatic mechanism for the regulation of mitochondrial clearance that is independent of splicing factor mutations. Prior work has established that, under basal conditions, PINK1 protein is degraded within mitochondria with a high MMP, whereas low MMP associated with mitochdonrial dysfunction allows PINK1 protein stabilization, accumulation at the outer membrane of mitochondira, and initiation of mitophagy[49]. The new homeostatic mechanism described here functions by altering *PINK1* splicing: mitochondrial dysfunction, whether caused by direct pharmacological disruption of the MMP or indirectly by the *SRSF2* mutation, promotes the excision of a poison intron to yield a more stable *PINK1* mRNA. The *SRSF2*^{P95*} mutation alters exonic binding site preferences for SRSF2 protein, leading to mis-splicing of key hematopoietic regulators such as *EZH2*[7]; thus *SRSF2*^{P95H} could directly alter the splicing of *PINK1* mRNA. However, SRSF2 typically regulates cassette exon selection whereas we observe enhanced intron excision and, importantly, CCCP alters *PINK1* splicing in cells with wild-type *SRSF2,* supporting a homeostatic mechanism that is sensitive to but independent of the *SRSF2* mutation. Although the altered splicing of *PINK1* mRNA described here is distinct from the well-established regulation of PINK1 protein stability by MMP, both mechanisms result in increased PINK1 protein abundance under conditions of mitochondrial stress. Our data thus support a novel mechanism for sensing mitochondrial stress through modulation of *PINK1* splicing, increasing *PINK1* expression and mitophagy.

Splicing out of the poison intron requires GSK-3, which phosphorylates multiple core splicing factors and regulates splicing at a transcriptome-wide level in diverse cell types[21-25]. Thus, pharmacologic inhibition or *GSK3* knock out impairs splicing of *PINK1*, leading to retention of the poison intron and reduction in overall levels of *PINK1* mRNA and protein. Altered splicing of *PINK1* explains the lethality

of GSK-3 inhibitors in *SRSF2*$^{P95H/+}$ cells, as survival in the presence of a GSK-3 inhibitor is rescued by expression of *PINK1* cDNA. Furthermore, chloroquine, which targets autophagy downstream of *PINK1,* is also selectively lethal to *SRSF2*$^{P95H/+}$ cells, supporting the hypothesis that these splicing factor mutant cells are dependent on mitophagy for survival and suggesting an actionable therapeutic target in splicing factor mutant myeloid neoplasms.

Currently there are no FDA approved drugs targeting splicing factor mutant cells. Here we identify mitophagy as a new therapeutic vulnerability. We have also uncovered a mechanism for mitochondrial surveillance that is mediated through GSK-3-dependent alternative splicing of *PINK1* and show increased sensitivity to GSK-3 or autophagy inhibition in splicing factor mutant cells. Several GSK-3 inhibitors are either in wide clinical use or have been shown to be safe in phase I-III clinical trials[50-53] and could be repurposed to treat MDS. Hence targeting mitophagy with GSK-3 inhibitors or general autophagy inhibitors may provide a new opportunity to treat splicing factor mutant MDS and AML.

Acknowledgements

P.S.K. was supported by grants from the National Institutes of Health (R01HL141759; R56DK133258-01), the Leukemia and Lymphoma Society (#8036-23), and the Institute for Translational Medicine and Applied Therapeutics at the University of Pennsylvania. K.W.L. is supported by NIH grant #R35-GM118048. M.C.P. is supported by VA Merit Award I01BX004662. D.C.W. is supported by NIH grant #R01CA259635-01A1.

Author Contributions/CRediT statement: Conceptualization: X.L., P.S.K.; Methodology: X.L.,M.Q.V., N.S., M.P.C., R.M., K.J.; Supervision and funding acquisition: P.S.K., O.A.W., K.W.L., D.C.W.; Investigation: X.L., S.A.D., R.F.S., R.M., K.J., M.Q.V., O.P., A.A.M., C.L.; Resources: P.S.K., R.F.S., O.A.W., N.S., M.P.C., J.H., K.W.L., D.C.W.; Writing and editing: XL, PSK, RFS, RM, KJ, NS; Visualization: X.L.,O.P., A.A.M.; Supervision: P.S.K., O.A.W., K.W.L., D.C.W., M.P.C., J.H.; Funding acquisition: P.S.K.

Declaration of Interests: P.S.K. is collaborating with Blueprint Medicines under a sponsored research agreement unrelated to the current manuscript. O.A.-W. has served as a consultant for H3B Biomedicine, Foundation Medicine Inc., Merck, Prelude Therapeutics, and Janssen, and is on the Scientific Advisory Board of Envisagenics Inc., AIChemy, Harmonic Discovery Inc., and Pfizer Boulder; O.A.-W. has received prior research funding from H3B Biomedicine, Nurix Therapeutics, Minovia Therapeutics, and LOXO Oncology unrelated to the current manuscript. D.C.W. is on the scientific advisory boards of Pano Therapeutics and Medical Excellence Capital.

Methods

Cell lines, primary human samples, constructs and nucleofection

BM- or peripheral blood- derived MNCs from AML or CMML patients were obtained from the Stem Cell and Xenograft Core Facility at University of Pennsylvania (RRID: SCR_010035). Detailed patient characteristics are listed in Supplementary Table 1. $CD34^+$ cells were purified from CMML patients through immunomagnetic selection (Miltenyi Biotec) according to the manufacturer's instructions. $CD34^+$ cells from healthy donors were purchased from STEMCELL Technologies. Cryopreserved AML MNCs were resuspended in IMDM medium supplemented with 15% BIT (bovine serum albumin, insulin, transferrin, STEMCELL Technologies), 100ng/ml SCF, 50ng/ml FLT3L, 20ng/ml IL-3, and 20ng/ml G-CSF. $CD34^+$ cells enriched from CMML patients or healthy donors were cultured in StemSpan SFEM II medium (STEMCELL Technologies) supplemented with 10% fetal bovine serum (FBS), 1% L-glutamine, 10ng/ml IL-3, 10ng/ml IL-6, and 25ng/ml SCF. TF-1 cells were maintained in RPMI supplemented with 10% FBS and 2ng/ml hGC-SCF (PeproTech). K562 cells were cultured in IMDM supplemented with 10% FBS. Cells were maintained at 37°C and 5% CO_2. *PINK1* (pLenti6-DEST PINK1-V5 WT, 13320), *WT* (pRRL_SRSF2_WT_mCherry, 84020), and *P95H SRSF2* (pRRL_SRSF2_P95H_mCherry, 84023) lentiviral overexpression constructs were purchased from Addgene. Lentiviruses were produced and used to transduce TF-1, K562, and primary AML cells, as described previously[54]. HEK293T cells were cultured in DMEM supplemented with 10% FBS, and 1% penicillin/streptomycin. *GSK3A/B* DKO HEK293T cells were generated by lentiviral delivery of Cas9 and guide RNA sequence targeting *GSK-3A* (GCCTAGAGTGGCTACGACTG) and *GSK-3B* (AGATGAGGTCTATCTTAATC) followed by single clone selection as previously described[50]. *GSK3A/B* DKO HEK293T cells were transfected using Lipofectamine 3000 (Invitrogen) according to manufacturer's instructions.

Flow cytometry, apoptosis assay and cell cycle analysis

All FACS antibodies were purchased from BioLegend. For apoptosis assay, K562, TF-1, primary AML blast or $CD34^+$ cells purified from CMML patients or healthy donors were suspended in Annexin V Binding buffer and incubated with anti-Annexin V antibody and 7-AAD for 15 min at room temperature (RT) in the dark. Immunophenotypes of viable cells or cells in early apoptosis, or late apoptosis were defined as Annexin V^-7-AAD^-, Annexin V^+7-AAD^- or Annexin V^+7-AAD^+, respectively. For cell cycle analysis, cells were fixed and permeablized in 70% ethanol in -20°C for 1 h, washed in cold FACS buffer, and then stained with anti-Ki67 (BD) for 30 mins on ice. After staining, cells were washed twice in FACS buffer and resuspended in FACS buffer containing 10μM DAPI. Stained cells were then tested by flow cytometry.

Cell growth assay

Triplicates of WT and *SRSF2*$^{P95H/+}$ K562 cells were seeded at 10,000 cells per well in 96-well plates and treated with indicated concentrations of CHIR (Cayman, 13122) or Chloroquine (Sigma, C6628). Four days after culture, MTS reagent (Abcam, ab197010) was added to cell medium at a final concentration of 0.5 mg/mL for 3 h at 37°C, and cell viability was measured as per manufacture's instructions. IC_{50} was determined with GraphPad Prism 8 using baseline correction (by normalizing to vehicle control), the asymmetric (five parameter) equation and least squares fit.

Immunoblotting

Cells were lysed in RIPA buffer plus protease inhibitor cocktail (Sigma, P8340), phosphatase inhibitor cocktail #2 (Sigma, P5726) and #3 (Sigma, P0044) used 1:100 each. Supernatants were collected after

centrifugation at 14,000 rpm for 15 min at 4°C, adjusted to 1x laemmli sample buffer and subjected to SDS-PAGE and then immunoblotted as described previously[50]. Antibodies for biochemical studies were purchased from the following vendors: anti-GAPDH (2118), cleaved caspase 8 (9496), cleaved caspase 3 (9661), Flag-tag (14793), V5-tag (13202), and β-catenin (9562) were from Cell Signaling Technology. Other antibodies included antibodies to PINK1 (Invitrogen, PA5-86941) and β-actin (Sigma, A5441).

Real time qPCR and RT-PCR

RNA was extracted from TF-1, K562, and primary cells using Rneasy Kit (Qiagen) according to the manufacturer's instructions. cDNA was synthesized using the SuperScript III (Life Technologies) according to the manufacturer's instructions. For detection of PINK1 mature mRNA, the following primers were used: forward: 5'-GCCTCATCGAGGAAAAACAGG-3'; reverse: 5'-GTCTCGTGTCCAACGGGTC-3'. For detection of PINK1 pre-mRNA, the following primers were used: intron 5 forward: 5'-CCTTTGCCTGGGGATTTTGC-3'; intron 5 reverse: 5'-GGGGCTAATGGCTCAGTGTT-3'; Intron 1 forward: 5'-GAGGCGAGGGTCCTTAAAGC-3'; intron 1 reverse: 5'- TGCGACAGGAGCTGTAATCG-3'. For detection of the PINK1 aberrant junction, the following primers were used: forward: 5'-GGTGATCGCAGATTTTGGCT-3'; reverse: 5'-GCCCGAAGATTTCATAGGCG-3'. The primers used for *BCL-X* isoform specific real-time qPCR analysis: *BCL-X* all forward: 5'-CATCAATGGCAACCCATCCTG-3'; reverse: 5'-GCAGTTCAAACTCGTCGCCT-3'; *BCL-Xs* forward: 5'-GAGCTTTGAACAGGATACTTTTGTGG-3': reverse: 5'-TTCCGACTGAAGAGTGAGCC-3'. The primers used for *DEPDC1* isoform specific qPCR analysis: *DEPDC1* all forward: 5'-TGATGCAATGGGTACGAGGT-3'; reverse: 5'-TCTTCCAGCAAGAAGCTCATCA-3'; *DEPDC1* long isoform forward: 5'-GAACTCGGAGAGTCTAGTGCC-3': reverse: 5'-CATCGATGGCAACCCTCTCT -3'. Statistical comparison of the expression of mRNA isoforms as determined through qPCR data was performed using the Student's t-test.

Immunoflorecent staining for mitophagy measurement

WT and *SRSF2*$^{P95H/+}$ K562 cells cells were treated with DMSO or 3μM CHIR for 44 h, then seeded on poly-D-lysine coated slides for 4 h at 37°C. After incubation, cells were fixed with 4% paraformaldehyde (pH 7.4) for 15 mins, permeabilized with 0.1% Triton X-100 for 15 mins, and blocked with 2% bovine serum albumin in PBS for 1 h at room temperature. Cells were immunostained with mouse anti-TOMM20 antibody (1:100 dilution, clone 4F3, Sigma-Aldrich), rabbit anti-LAMP1 antibody (1:100 dilution, A2582, ABclonal) overnight at 4°C in a humidified chamber. Secondary antibodies in anti-rabbit AF568 and anti-mouse AF488 (1:100 dilution) were incubated at room temperature for 60 mins. The slides were then air-dried in dark at room temperature for 10 minutes and mounted in anti-fade mounting medium (Abcam, ab104135) before confocal imaging. Co-localization of TOMM20 and LAMP1 was quantified with JaCoP plug-in in Fiji.

Measurements of mitochondrial mass, membrane potential and mitochondrial DNA copy number

For mitochondrial mass measurement, cells were stained with 15nM Mitotracker green for 20 mins at room temperature in dark followed by flow cytometric analysis. For mitochondrial membrane potential analysis, cells were stained with 200nM TMRE for 20 mins at room temperature. JC-1 staining was used for detect mitochondrial depolarization occurring in apoptosis. WT and *SRSF2*$^{P95H/+}$ K562 cells

were treated with or without 2μM CCCP for 24h, and then stained with 1μM JC-1 for 20 mins. To quantify mitochondrial DNA copy number, quantitative PCR was performed with primers for mitochondrial mt-ND1 (Forward: GCAGAGACCAACCGAACCCCC; Reverse: GGGCCTGCGGCGTATTCGAT) and nuclear β2 microglobulin (B2M) (Forward: GCAGAGACCAACCGAACCCCC; Reverse: GGCGGGCCACCAAGGAGAAC).

Transmission electron microscopy

K562 WT and *SRSF2*$^{P95H/+}$ cells for electron microscopic examination were fixed with 2.5% glutaraldehyde, 2.0% paraformaldehyde in 0.1M sodium cacodylate buffer, pH7.4, overnight at 4°C. After subsequent buffer washes, the samples were post-fixed in 2.0% osmium tetroxide for 1 hour at room temperature, and rinsed in dH_2O prior to en bloc staining with 2% uranyl acetate. After dehydration through a graded ethanol series, the tissue was infiltrated and embedded in EMbed-812 (Electron Microscopy Sciences, Fort Washington, PA). Thin sections were stained with uranyl acetate and lead citrate and examined with a JEOL1010 electron microscope fitted with a Hamamatsu digital camera and AMT Advantage image capture software. Images of single cells were saved as separate image files and an observer blind to the identity of each cell counted vesicles per cell.

Measurement of mitochondrial respiration

Oxygen consumption was measured using high-resolution respirometry Oxygraph-2k (Oroboros Instruments, Innsbruck, Austria) with a polarographic oxygen electrode and two 2-mL chambers allowing for parallel measurements[52]. Briefly, K562 WT and *SRSF2*$^{P95H/+}$ cells in MiR05 buffer (0.5mM EGTA, 3mM MgCl2, 60mM lactobionic acid, 20mM taurine, 10mM KH2PO4, 20mM HEPES, 110 mM D-sucrose, 1g/L BSA) were added into the closed chamber through a small capillary tube. Oxygen concentration (μmol/L) and oxygen flux [pmol/(s×Mill)] were simultaneously recorded in real-time. During the assay, 5ug/ml Digitonin, 5mM Pyruvate, 2mM Malate, 10mM Glutamate, 2.5mM ADP, 5nM Oligomycin, 0.5uM FCCP, 0.5uM Rotenone, and 2.5uM Antimycin A were added sequentially.

K562 xenograft model

$5X10^6$ K562 WT or *SRSF2*$^{P95H/+}$ cells were subcutaneously implanted into the flank of female NSG mice of 6–8 weeks of age. Mice were then treated with 30mg/kg body weight CHIR or vehicle (10% DMSO, 45% PEG400, and 45% PBS, injected subcutaneously) daily for the duration of the implantation period. Tumor size was measured three times a week using a caliper. Tumor volume was calculated by using the ellipsoid formula: (length X width2)/2. All mouse studies were carried out under protocol approved by the Upenn Guide for the Care and Use of Laboratory Animals.

RNA-seq sample preparation

K562 isogenic lines were treated with 3μM CHIR for 24 h. After treatment, the cells were washed with cold PBS, and RNA was isolated using Rneasy Kit (Qiagen) according to the manufacturer's instructions. cDNA library preparation, sequencing, and raw read filtering methods were described previously[21].

Quantification of RNA-seq data

Raw sequence reads were aligned to the human reference sequence hg38 by STAR 2.4.2a using two-pass alignment. Raw gene counts were compiled into total gene counts, then analyzed using EdgeR

3.20.2 to assess the significance of changes between cohorts. Gene changes with a padj value < 0.05 were considered significant. Significant gene expression changes are provided in Supplementary Table 2. Heatmaps for BCL2 family gene expression and mitophagy related genes expression were generated by using Morpheus tool (Borad Institute, https://software.broadinstitute.org/morpheus/). Briefly, normalized expression values were transformed to z-scored log2 expression by subtracting row mean and then dividing by row standard deviation. RNA-seq data were deposited in the NCBI Gene Expression Omnibus[55] and are accessible through GEO Series accession number GSE235600, https://www.ncbi.nlm.nih.gov/geo/query/acc.cgi?acc=GSE235600.

Identification of differential splicing events

Alternative splicing analyses relied on RNA-Seq reads mapped to the reference human genome as described using rMATS v4.1.1 with the default parameters[30]. Events were defined as significant if (1) the FDR corrected p value was smaller than 0.05 and (2) dPSI was larger than 10%. Examples of splicing and mis-splicing events were visualized with IGV (Broad Institute). Heatmap for alternative splicing events between *WT* or *SRSF2*$^{P95H/+}$ cells was generated by using Morpheus. Hierarchical clustering was performed using metric one minus person correlation.

Gene ontology analysis

Gene set enrichment was performed using Metascape (https://metascape.org) using the KEGG, and GO specific signatures according to the manual.

GSEA analysis

GSEA analysis was performed using GSEA version 4.3 (Broad). Normalized reads values produced from gene expression analysis were formatted into GCT files containing expression values for genes in different biological states. CLS files were manually built to label biological states involved in each study. Following parameters were used: Number of permutations = 1000, permutation type = gene_set, chip platform = human_Ensembl_gene_ID_MSigDB.v2023.1.chip. Other parameters were used at default values.

Mass spectrometry

SRSF2$^{+/+}$ (*WT)* and *SRSF2*$^{P95H/+}$ K562 cell pellets were resuspended in a solution of 100 mM ammonium bicarbonate and 8 M urea. Samples were sonicated for 15 sec then placed on ice for 15 sec ten times, and then were centrifuged at 20,000xg for 5 min at 4°C. Protein concentration in supernatants was measured by BCA assay. For each sample, 100 µg of protein was diluted to 50 µL at a final concentration of 10 mM DTT and incubated at 56°C for 30 min to reduce cystines to cysteines. Alkylation was performed by adding 5.5 µL of 0.5 M iodoacetamide and incubating at RT in the dark for 40 minutes. Samples were diluted to 250 µL with 50 mM Tris-HCl (pH 8.3), 2 µg of sequencing grade modified trypsin (Promega) was added, and samples were incubated at 37°C overnight. Samples were acidified to 0.1% trifluoroacetic acid (TFA) and immediately desalted using C18 stagetips, washing with 0.1% formic acid and eluting with 0.1% formic acid in 60% acetonitrile (ACN). Peptides were dried in a Savant SpeedVac and then resuspended in 20 uL of 0.1% trifluoroacetic acid (TFA). UV absorption at 280 nm (A280) was measured to normalize injection volumes and samples were run on a Dionex UltiMate 3000 nanoLC and Q Exactive HF (Thermo Scientific). Peptides were loaded on a C18 trap column (Thermo Scientific), washed with buffer A (0.1% formic acid) and then separated using an

analytical column (75 µm x 15 cm) packed in-house with C18 resin (Dr. Maisch, GMBH), using an analytical gradient of 5% buffer B (0.1% formic acid in 80% ACN) to 25% over 90 min, and then 25% to 45% over 30 min. MS detection was performed using data independent acquisition with 24 *m/z* windows. Data were searched using DIA-NN with a UniProt FASTA digest library-free search and without heuristic protein inference. The mass spectrometry proteomics data have been deposited to the ProteomeXchange Consortium via the PRIDE[56] partner repository with the dataset identifier PXD043213.

AML TCGA analysis

Gene expression analysis of *OPTN*, *ULK1* and *TOMM7* in AML patients from the TCGA project[57] was retrieved from cBioportal for Cancer Genomics (https://www.cbioportal.org)[58], and visualized using Prism (GraphPad). GEPIA (http://gepia.cancer-pku.cn) was used for overall survival (OS) analysis based on high and low expression of *OPTN* in publicly available TCGA datasets.

Statistics

Statistical analysis was performed using Prism version 8 software. Unless otherwise specified, statistical differences between two groups were determined by 2-tailed Student's *t* test. $P < 0.05$ was considered significant.

References

1. Kim, Y.J., and Abdel-Wahab, O. (2017). Therapeutic targeting of RNA splicing in myelodysplasia. Semin Hematol *54*, 167-173. 10.1053/j.seminhematol.2017.06.007.
2. Dvinge, H., Kim, E., Abdel-Wahab, O., and Bradley, R.K. (2016). RNA splicing factors as oncoproteins and tumour suppressors. Nature reviews. Cancer *16*, 413-430. 10.1038/nrc.2016.51.
3. Yoshida, K., Sanada, M., Shiraishi, Y., Nowak, D., Nagata, Y., Yamamoto, R., Sato, Y., Sato-Otsubo, A., Kon, A., Nagasaki, M., et al. (2011). Frequent pathway mutations of splicing machinery in myelodysplasia. Nature *478*, 64-69. 10.1038/nature10496.
4. Papaemmanuil, E., Cazzola, M., Boultwood, J., Malcovati, L., Vyas, P., Bowen, D., Pellagatti, A., Wainscoat, J.S., Hellstrom-Lindberg, E., Gambacorti-Passerini, C., et al. (2011). Somatic SF3B1 mutation in myelodysplasia with ring sideroblasts. The New England journal of medicine *365*, 1384-1395. 10.1056/NEJMoa1103283.
5. Graubert, T.A., Shen, D., Ding, L., Okeyo-Owuor, T., Lunn, C.L., Shao, J., Krysiak, K., Harris, C.C., Koboldt, D.C., Larson, D.E., et al. (2011). Recurrent mutations in the U2AF1 splicing factor in myelodysplastic syndromes. Nature genetics *44*, 53-57. 10.1038/ng.1031.
6. Inoue, D., Bradley, R.K., and Abdel-Wahab, O. (2016). Spliceosomal gene mutations in myelodysplasia: molecular links to clonal abnormalities of hematopoiesis. Genes & development *30*, 989-1001. 10.1101/gad.278424.116.
7. Kim, E., Ilagan, J.O., Liang, Y., Daubner, G.M., Lee, S.C., Ramakrishnan, A., Li, Y., Chung, Y.R., Micol, J.B., Murphy, M.E., et al. (2015). SRSF2 Mutations Contribute to Myelodysplasia by Mutant-Specific Effects on Exon Recognition. Cancer Cell *27*, 617-630. 10.1016/j.ccell.2015.04.006.
8. Rivera, O.D., Mallory, M.J., Quesnel-Vallieres, M., Chatrikhi, R., Schultz, D.C., Carroll, M., Barash, Y., Cherry, S., and Lynch, K.W. (2021). Alternative splicing redefines landscape of commonly mutated genes in acute myeloid leukemia. Proceedings of the National Academy of Sciences of the United States of America *118*. 10.1073/pnas.2014967118.
9. Pellagatti, A., Armstrong, R.N., Steeples, V., Sharma, E., Repapi, E., Singh, S., Sanchi, A., Radujkovic, A., Horn, P., Dolatshad, H., et al. (2018). Impact of spliceosome mutations on RNA splicing in myelodysplasia: dysregulated genes/pathways and clinical associations. Blood *132*, 1225-1240. 10.1182/blood-2018-04-843771.
10. Bejar, R., Stevenson, K.E., Caughey, B.A., Abdel-Wahab, O., Steensma, D.P., Galili, N., Raza, A., Kantarjian, H., Levine, R.L., Neuberg, D., et al. (2012). Validation of a prognostic model and the impact of mutations in patients with lower-risk myelodysplastic syndromes. Journal of clinical oncology : official journal of the American Society of Clinical Oncology *30*, 3376-3382. 10.1200/JCO.2011.40.7379.
11. Patnaik, M.M., and Tefferi, A. (2016). Cytogenetic and molecular abnormalities in chronic myelomonocytic leukemia. Blood cancer journal *6*, e393. 10.1038/bcj.2016.5.
12. Lee, S.C., Dvinge, H., Kim, E., Cho, H., Micol, J.B., Chung, Y.R., Durham, B.H., Yoshimi, A., Kim, Y.J., Thomas, M., et al. (2016). Modulation of splicing catalysis for therapeutic targeting of leukemia with mutations in genes encoding spliceosomal proteins. Nature medicine *22*, 672-678. 10.1038/nm.4097.
13. Wang, E., Lu, S.X., Pastore, A., Chen, X., Imig, J., Chun-Wei Lee, S., Hockemeyer, K., Ghebrechristos, Y.E., Yoshimi, A., Inoue, D., et al. (2019). Targeting an RNA-Binding Protein Network in Acute Myeloid Leukemia. Cancer Cell *35*, 369-384 e367. 10.1016/j.ccell.2019.01.010.
14. Steensma, D.P., Wermke, M., Klimek, V.M., Greenberg, P.L., Font, P., Komrokji, R.S., Yang, J., Brunner, A.M., Carraway, H.E., Ades, L., et al. (2021). Phase I First-in-Human Dose Escalation

Study of the oral SF3B1 modulator H3B-8800 in myeloid neoplasms. Leukemia. 10.1038/s41375-021-01328-9.
15. Hsu, T.Y., Simon, L.M., Neill, N.J., Marcotte, R., Sayad, A., Bland, C.S., Echeverria, G.V., Sun, T., Kurley, S.J., Tyagi, S., et al. (2015). The spliceosome is a therapeutic vulnerability in MYC-driven cancer. Nature *525*, 384-388. 10.1038/nature14985.
16. Crews, L.A., Balaian, L., Delos Santos, N.P., Leu, H.S., Court, A.C., Lazzari, E., Sadarangani, A., Zipeto, M.A., La Clair, J.J., Villa, R., et al. (2016). RNA Splicing Modulation Selectively Impairs Leukemia Stem Cell Maintenance in Secondary Human AML. Cell stem cell *19*, 599-612. 10.1016/j.stem.2016.08.003.
17. Shirai, C.L., Tripathi, M., Ley, J.N., Ndonwi, M., White, B.S., Tapia, R., Saez, B., Bertino, A., Shao, J., Kim, S., et al. (2015). Preclinical Activity of Splicing Modulators in U2AF1 Mutant MDS/AML. Blood *126*, 1653.
18. Seiler, M., Yoshimi, A., Darman, R., Chan, B., Keaney, G., Thomas, M., Agrawal, A.A., Caleb, B., Csibi, A., Sean, E., et al. (2018). H3B-8800, an orally available small-molecule splicing modulator, induces lethality in spliceosome-mutant cancers. Nature medicine *24*, 497-504. 10.1038/nm.4493.
19. Liu, X., and Klein, P.S. (2018). Glycogen synthase kinase-3 and alternative splicing. Wiley Interdiscip Rev RNA *9*, e1501. 10.1002/wrna.1501.
20. Guezguez, B., Almakadi, M., Benoit, Y.D., Shapovalova, Z., Rahmig, S., Fiebig-Comyn, A., Casado, F.L., Tanasijevic, B., Bresolin, S., Masetti, R., et al. (2016). GSK3 Deficiencies in Hematopoietic Stem Cells Initiate Pre-neoplastic State that Is Predictive of Clinical Outcomes of Human Acute Leukemia. Cancer Cell *29*, 61-74. 10.1016/j.ccell.2015.11.012.
21. Shinde, M.Y., Sidoli, S., Kulej, K., Mallory, M.J., Radens, C.M., Reicherter, A.L., Myers, R.L., Barash, Y., Lynch, K.W., Garcia, B.A., and Klein, P.S. (2017). Phosphoproteomics reveals that glycogen synthase kinase-3 phosphorylates multiple splicing factors and is associated with alternative splicing. The Journal of biological chemistry *292*, 18240-18255. 10.1074/jbc.M117.813527.
22. Heyd, F., and Lynch, K.W. (2010). Phosphorylation-dependent regulation of PSF by GSK3 controls CD45 alternative splicing. Molecular cell *40*, 126-137. 10.1016/j.molcel.2010.09.013.
23. Hernandez, F., Perez, M., Lucas, J.J., Mata, A.M., Bhat, R., and Avila, J. (2004). Glycogen synthase kinase-3 plays a crucial role in tau exon 10 splicing and intranuclear distribution of SC35. Implications for Alzheimer's disease. The Journal of biological chemistry *279*, 3801-3806. 10.1074/jbc.M311512200.
24. Wang, S.B., Venkatraman, V., Crowgey, E.L., Liu, T., Fu, Z., Holewinski, R., Ranek, M., Kass, D.A., O'Rourke, B., and Van Eyk, J.E. (2018). Protein S-Nitrosylation Controls Glycogen Synthase Kinase 3beta Function Independent of Its Phosphorylation State. Circulation research *122*, 1517-1531. 10.1161/CIRCRESAHA.118.312789.
25. Martinez, N.M., Agosto, L., Qiu, J., Mallory, M.J., Gazzara, M.R., Barash, Y., Fu, X.D., and Lynch, K.W. (2015). Widespread JNK-dependent alternative splicing induces a positive feedback loop through CELF2-mediated regulation of MKK7 during T-cell activation. Genes & development *29*, 2054-2066. 10.1101/gad.267245.115.
26. Lee, S.C., North, K., Kim, E., Jang, E., Obeng, E., Lu, S.X., Liu, B., Inoue, D., Yoshimi, A., Ki, M., et al. (2018). Synthetic Lethal and Convergent Biological Effects of Cancer-Associated Spliceosomal Gene Mutations. Cancer Cell *34*, 225-241 e228. 10.1016/j.ccell.2018.07.003.
27. Larrayoz, M., Blakemore, S.J., Dobson, R.C., Blunt, M.D., Rose-Zerilli, M.J., Walewska, R., Duncombe, A., Oscier, D., Koide, K., Forconi, F., et al. (2016). The SF3B1 inhibitor spliceostatin A (SSA) elicits apoptosis in chronic lymphocytic leukaemia cells through downregulation of Mcl-1. Leukemia *30*, 351-360. 10.1038/leu.2015.286.
28. Moore, M.J., Wang, Q., Kennedy, C.J., and Silver, P.A. (2010). An alternative splicing network links cell-cycle control to apoptosis. Cell *142*, 625-636. 10.1016/j.cell.2010.07.019.

29. Aird, D., Teng, T., Huang, C.L., Pazolli, E., Banka, D., Cheung-Ong, K., Eifert, C., Furman, C., Wu, Z.J., Seiler, M., et al. (2019). Sensitivity to splicing modulation of BCL2 family genes defines cancer therapeutic strategies for splicing modulators. Nat Commun *10*, 137. 10.1038/s41467-018-08150-5.
30. Shen, S., Park, J.W., Lu, Z.X., Lin, L., Henry, M.D., Wu, Y.N., Zhou, Q., and Xing, Y. (2014). rMATS: robust and flexible detection of differential alternative splicing from replicate RNA-Seq data. Proceedings of the National Academy of Sciences of the United States of America *111*, E5593-5601. 10.1073/pnas.1419161111.
31. Darman, R.B., Seiler, M., Agrawal, A.A., Lim, K.H., Peng, S., Aird, D., Bailey, S.L., Bhavsar, E.B., Chan, B., Colla, S., et al. (2015). Cancer-Associated SF3B1 Hotspot Mutations Induce Cryptic 3' Splice Site Selection through Use of a Different Branch Point. Cell reports *13*, 1033-1045. 10.1016/j.celrep.2015.09.053.
32. Lazarou, M., Sliter, D.A., Kane, L.A., Sarraf, S.A., Wang, C., Burman, J.L., Sideris, D.P., Fogel, A.I., and Youle, R.J. (2015). The ubiquitin kinase PINK1 recruits autophagy receptors to induce mitophagy. Nature *524*, 309-314. 10.1038/nature14893.
33. Glytsou, C., Chen, X., Zacharioudakis, E., Al-Santli, W., Zhou, H., Nadorp, B., Lee, S., Lasry, A., Sun, Z., Papaioannou, D., et al. (2023). Mitophagy promotes resistance to BH3 mimetics in acute myeloid leukemia. Cancer Discov. 10.1158/2159-8290.CD-22-0601.
34. Vannucchi, A.M., Lasho, T.L., Guglielmelli, P., Biamonte, F., Pardanani, A., Pereira, A., Finke, C., Score, J., Gangat, N., Mannarelli, C., et al. (2013). Mutations and prognosis in primary myelofibrosis. Leukemia *27*, 1861-1869. 10.1038/leu.2013.119.
35. Wu, S.J., Kuo, Y.Y., Hou, H.A., Li, L.Y., Tseng, M.H., Huang, C.F., Lee, F.Y., Liu, M.C., Liu, C.W., Lin, C.T., et al. (2012). The clinical implication of SRSF2 mutation in patients with myelodysplastic syndrome and its stability during disease evolution. Blood *120*, 3106-3111. 10.1182/blood-2012-02-412296.
36. Zhang, S.J., Rampal, R., Manshouri, T., Patel, J., Mensah, N., Kayserian, A., Hricik, T., Heguy, A., Hedvat, C., Gonen, M., et al. (2012). Genetic analysis of patients with leukemic transformation of myeloproliferative neoplasms shows recurrent SRSF2 mutations that are associated with adverse outcome. Blood *119*, 4480-4485. 10.1182/blood-2011-11-390252.
37. Papaemmanuil, E., Gerstung, M., Malcovati, L., Tauro, S., Gundem, G., Van Loo, P., Yoon, C.J., Ellis, P., Wedge, D.C., Pellagatti, A., et al. (2013). Clinical and biological implications of driver mutations in myelodysplastic syndromes. Blood *122*, 3616-3627; quiz 3699. 10.1182/blood-2013-08-518886.
38. Yoshimi, A., Lin, K.T., Wiseman, D.H., Rahman, M.A., Pastore, A., Wang, B., Lee, S.C., Micol, J.B., Zhang, X.J., de Botton, S., et al. (2019). Coordinated alterations in RNA splicing and epigenetic regulation drive leukaemogenesis. Nature *574*, 273-277. 10.1038/s41586-019-1618-0.
39. Salvioli, S., Ardizzoni, A., Franceschi, C., and Cossarizza, A. (1997). JC-1, but not DiOC6(3) or rhodamine 123, is a reliable fluorescent probe to assess delta psi changes in intact cells: implications for studies on mitochondrial functionality during apoptosis. FEBS letters *411*, 77-82. 10.1016/s0014-5793(97)00669-8.
40. Ito, K., Turcotte, R., Cui, J., Zimmerman, S.E., Pinho, S., Mizoguchi, T., Arai, F., Runnels, J.M., Alt, C., Teruya-Feldstein, J., et al. (2016). Self-renewal of a purified Tie2+ hematopoietic stem cell population relies on mitochondrial clearance. Science *354*, 1156-1160. 10.1126/science.aaf5530.
41. Ayyathan, D.M., Sharon, D., Cathelin, S., and Chan, S.M. (2021). Inhibition of PINK1-Dependent Mitochondrial Quality Control Pathways Induces Senescence of Acute Myeloid Leukemia Stem Cells. Blood Supplement (abstract) *138*, 2225.
42. Pei, S., Minhajuddin, M., Adane, B., Khan, N., Stevens, B.M., Mack, S.C., Lai, S., Rich, J.N., Inguva, A., Shannon, K.M., et al. (2018). AMPK/FIS1-Mediated Mitophagy Is Required for Self-

Renewal of Human AML Stem Cells. Cell stem cell *23*, 86-100 e106. 10.1016/j.stem.2018.05.021.
43. Juhaszova, M., Zorov, D.B., Kim, S.H., Pepe, S., Fu, Q., Fishbein, K.W., Ziman, B.D., Wang, S., Ytrehus, K., Antos, C.L., et al. (2004). Glycogen synthase kinase-3beta mediates convergence of protection signaling to inhibit the mitochondrial permeability transition pore. The Journal of clinical investigation *113*, 1535-1549. 10.1172/JCI19906.
44. Nguyen-McCarty, M., and Klein, P.S. (2017). Autophagy is a signature of a signaling network that maintains hematopoietic stem cells. PloS one *12*, e0177054. 10.1371/journal.pone.0177054.
45. Mossner, M., Jann, J.C., Wittig, J., Nolte, F., Fey, S., Nowak, V., Oblander, J., Pressler, J., Palme, I., Xanthopoulos, C., et al. (2016). Mutational hierarchies in myelodysplastic syndromes dynamically adapt and evolve upon therapy response and failure. Blood *128*, 1246-1259. 10.1182/blood-2015-11-679167.
46. Cancer Genome Atlas Research, N. (2013). Genomic and epigenomic landscapes of adult de novo acute myeloid leukemia. The New England journal of medicine *368*, 2059-2074. 10.1056/NEJMoa1301689.
47. Vannini, N., Campos, V., Girotra, M., Trachsel, V., Rojas-Sutterlin, S., Tratwal, J., Ragusa, S., Stefanidis, E., Ryu, D., Rainer, P.Y., et al. (2019). The NAD-Booster Nicotinamide Riboside Potently Stimulates Hematopoiesis through Increased Mitochondrial Clearance. Cell stem cell *24*, 405-418 e407. 10.1016/j.stem.2019.02.012.
48. Mattes, K., Vellenga, E., and Schepers, H. (2019). Differential redox-regulation and mitochondrial dynamics in normal and leukemic hematopoietic stem cells: A potential window for leukemia therapy. Crit Rev Oncol Hematol *144*, 102814. 10.1016/j.critrevonc.2019.102814.
49. Durcan, T.M., and Fon, E.A. (2015). The three 'P's of mitophagy: PARKIN, PINK1, and post-translational modifications. Genes & development *29*, 989-999. 10.1101/gad.262758.115.
50. Liu, X., Verma, A., Garcia, G., Ramage, H., Myers, R.L., Lucas, A., Michaelson, J.J., Coryell, W., Kumar, A., Charney, A.W., et al. (2021). Targeting the Coronavirus Nucleocapsid Protein through GSK-3 Inhibition. medRxiv. 10.1101/2021.02.17.21251933.
51. Bourhill, T., Narendran, A., and Johnston, R.N. (2017). Enzastaurin: A lesson in drug development. Crit Rev Oncol Hematol *112*, 72-79. 10.1016/j.critrevonc.2017.02.003.
52. Sanchez-Cruz, A., Martinez, A., de la Rosa, E.J., and Hernandez-Sanchez, C. (2019). GSK-3 Inhibitors: From the Brain to the Retina and Back Again. Advances in experimental medicine and biology *1185*, 437-441. 10.1007/978-3-030-27378-1_72.
53. Odia, Y., Cavalcante, L., Safran, H., Powell, S.F., Munster, P.N., Ma, W.W., Carneiro, B.A., Bastos, B.R., Mikrut, S., Mikrut, W., et al. (2022). Malignant glioma subset from actuate 1801: Phase I/II study of 9-ING-41, GSK-3beta inhibitor, monotherapy or combined with chemotherapy for refractory malignancies. Neurooncol Adv *4*, vdac012. 10.1093/noajnl/vdac012.
54. Hou, P., Chen, S., Wang, S., Yu, X., Chen, Y., Jiang, M., Zhuang, K., Ho, W., Hou, W., Huang, J., and Guo, D. (2015). Genome editing of CXCR4 by CRISPR/cas9 confers cells resistant to HIV-1 infection. Sci Rep *5*, 15577. 10.1038/srep15577.
55. Edgar, R., Domrachev, M., and Lash, A.E. (2002). Gene Expression Omnibus: NCBI gene expression and hybridization array data repository. Nucleic acids research *30*, 207-210. 10.1093/nar/30.1.207.
56. Perez-Riverol, Y., Bai, J., Bandla, C., Garcia-Seisdedos, D., Hewapathirana, S., Kamatchinathan, S., Kundu, D.J., Prakash, A., Frericks-Zipper, A., Eisenacher, M., et al. (2022). The PRIDE database resources in 2022: a hub for mass spectrometry-based proteomics evidences. Nucleic acids research *50*, D543-D552. 10.1093/nar/gkab1038.
57. Tyner, J.W., Tognon, C.E., Bottomly, D., Wilmot, B., Kurtz, S.E., Savage, S.L., Long, N., Schultz, A.R., Traer, E., Abel, M., et al. (2018). Functional genomic landscape of acute myeloid leukaemia. Nature *562*, 526-531. 10.1038/s41586-018-0623-z.

58. Cerami, E., Gao, J., Dogrusoz, U., Gross, B.E., Sumer, S.O., Aksoy, B.A., Jacobsen, A., Byrne, C.J., Heuer, M.L., Larsson, E., et al. (2012). The cBio cancer genomics portal: an open platform for exploring multidimensional cancer genomics data. Cancer Discov *2*, 401-404. 10.1158/2159-8290.CD-12-0095.

Figure Legends

Figure 1. Preferential cytotoxicity of GSK-3i in SF-mutant leukemia over WT counterparts (A) *WT, SRSF2*$^{P95H/+}$ and *SF3B1*$^{K700E/+}$ cells were cultured with DMSO or 3uM CHIR, and cell numbers were counted at 2 d and 4 d. (B) Percentages of viable, early-, and late-apoptotic cells based on 7-AAD and Annexin V flow cytometric analysis of isogenic K562 *WT*, *SRSF2*$^{P95H/+}$ and *SF3B1*$^{K700E/+}$ cells treated with DMSO or 3uM CHIR *in vitro* for 4 d (mean ± SD). Statistical analysis of viable fraction in mutant cells treated with CHIR relative to *wt* conterparts was performed using unpaired Student's t test. (C) K562 *WT*, *SRSF2*$^{P95H/+}$ and *SF3B1*$^{K700E/+}$ cells treated with vehicle or 3uM CHIR for 2 d were examined for cleaved caspase 3 and 8 expression by western blot (left). Bar graphs show relative levels of cleaved caspase 8 determined by densitometric analysis and normalized to GAPDH (right). (D) *WT* and *SF3B1*$^{K700E/+}$ cells were cultured with vehicle, 40uM caspase 8 inhibitor ZIETD, or 40uM pan-caspase inhibitor ZVAD and then treated with DMSO or 3uM CHIR. Apoptosis was measured by flow cytometric analysis as in Fig 1b. (E) Percentages of viable, early-, and late-apoptotic cells of K562 parental, *SRSF2*^{wt}-, or *SRSF2*^{P95H}-overexprssing cells treated with vehicle or 3uM CHIR *in vitro* for 4 d (mean ± SD). Statistical analysis of viable fraction in *SRSF2*^{P95H}-overexpressing cells treated with CHIR relative to *SRSF2*^{wt} conterparts was performed using unpaired Student's t test. (F) Schematic of *in vivo* K562 xenograft experiment. (G) Mean tumor volume in NSG mice subcutaneously implanted with K562 isogenic *WT* or *SRSF2*$^{P95H/+}$ cells. Mice received subcutaneous injections of vehicle or CHIR (30mg/kg) daily. Mean tumor volumes ± s.e.m. are shown.

Figure 2. Selective cytotoxicity of GSK-3i in primary human leukemia cells with SF mutations (A) CHIR induced higher levels of apoptosis in splicing factor mutant (mut) cells from patients with CMML (red) or AML (purple) compared to patients with *wt* splicing factors or CD34^{+} cells from healthy donors. Log2[fold change] in apoptosis in CHIR relative to DMSO treated is shown. Statistical analysis was performed using one-tailed Mann Whitney test. (B) Schematic of lentivirus infection in primary AML cells for apoptosis assay. (C) Primary AML cells from 3 patients were transduced with lentivirus encoding *WT* or mutant *SRSF2* as in panel B and cultured in the absence or presence of 3uM CHIR (blue box indicates duration of drug treatment). The percentage of mCherry^{+} cells normalized to the number at day 3 (patients 1 and 2) or day 4 (patient 3) is shown (mean ± SD). **: $p<0.01$. (D) Representive flow cytometric analysis (left) and quantification (right) of apoptosis in primary cells from patients with AML overexpressing either *SRSF2*$^{+}$ or *SRSF2*^{P95H}, as measured by Annexin V and 7-AAD staining in absence or presence of 3uM CHIR.

Figure 3. GSK-3i is associated with global alterations in gene expression and splicing in human leukemic cells (A) Schematic of deep RNA-Seq in *WT*, *SRSF2*$^{P95H/+}$ and *SF3B1*$^{K700E/+}$ K562 cells treated with DMSO or 3uM CHIR for 24 h. (B) Bar graphs show numbers of differential splicing events (FDR<0.05, dPSI>10%) in *WT*, *SRSF2*$^{P95H/+}$ and *SF3B1*$^{K700E/+}$ K562 cells treated with CHIR versus DMSO controls. A3SS, alternative 3' splice site; A5SS, alternative 5' splice site; MXE, mutually exclusive exon; RI, retained intron; SE, skipped exon. (C) Venn diagram showing the number of overlapping alternatively spliced genes between CHIR and DMSO in *wt*, *SRSF2*$^{P95H/+}$ and *SF3B1*$^{K700E/+}$ K562 cells. (D) Scatterplots of cassette exon inclusion in *WT*, *SRSF2*$^{P95H/+}$ and *SF3B1*$^{K700E/+}$ K562 cells treated with 3uM CHIR relative to DMSO treated controls. Brown (left) and purple (right) indicate cassette exons whose inclusion is repressed or promoted, respectively, in CHIR treated relative to

DMSO treated cells. (E) Bar graphs show numbers of alternative 3' splice site events upon CHIR treatment compared to DMSO in *WT*, *SRSF2*$^{P95H/+}$ and *SF3B1*$^{K700E/+}$ K562 cells. Purple and orange indicate intron-proximal 3' splice sites whose usage is repressed or enhanced, respectively, in CHIR treated relative to DMSO treated cells. (F) Sashimi plots of *DEPDC1* in *WT* and *SRSF2*$^{P95H/+}$ cells treated with DMSO or CHIR (left). Bar plots shows quantification of percentage of exon inclusion based on rMATS analysis (top right) and on isoform specific qPCR validation (bottom right). Percentage of exon inclusion was quantified by RT-qPCR analysis of mRNA levels containing the cassette exons normalized to total mRNA levels. ns: not significant.

Figure 4. GSK-3 regulates *PINK1* splicing (A) Venn diagram of genes differentially expressed (blue) or differentially spliced (green) in CHIR-treated *WT*, *SRSF2*$^{P95H/+}$ and *SF3B1*$^{K700E/+}$ K562 cells relative to DMSO-treated controls. (B) Sashimi plots of *PINK1* in *WT*, *SRSF2*$^{P95H/+}$ and *SF3B1*$^{K700E/+}$ cells treated with DMSO or CHIR (left). Bar graph shows intron 6 retention as a percentage of total transcripts (right). (C) *PINK1* mRNA levels in *WT*, *SRSF2*$^{P95H/+}$ and *SF3B1*$^{K700E/+}$ cells treated with DMSO or 3uM CHIR for 24 h detected by RT-qPCR using primers that span exons 1 and 2 (mean ± SD, n = 3). **: $p<0.001$. (D) *PINK1* nascent transcript detection by RT-qPCR using primers for intron 1 (left) and intron 5 (right) in *WT*, *SRSF2*$^{P95H/+}$ and *SF3B1*$^{K700E/+}$ cells treated with DMSO or 3uM CHIR for 24 h. (E-F) Representive RT-PCR with primers spanning exon 6 (E6), intron 6 (I6), and exon 7 (E7) of *PINK1* in *WT*, *SRSF2*$^{P95H/+}$, *SF3B1*$^{K700E/+}$ K562 cells (E) and primary AML cells, CD34^{+} cells from healthy donors, and CD34^{+} cells from CMML patients (F) treated with DMSO or 3uM CHIR for 24h. M: DNA marker. PCR product with retained intron 6 is 568bp and product for spliced exon6-7 (without retained intron) is 206bp. (G) RT-PCR analysis of *PINK1* splicing in *WT*, *GSK3A/B* DKO, and *GSK3A/B* DKO cells overexpressing GSK-3β (HEK293T).

Figure 5. *SRSF2*^{P95H} increases *PINK1* expression and mitophagy (A) Heat map shows z-scored expression of mitophagy related genes in *WT* and *SRSF2*$^{P95H/+}$ K562 cells. (B) Representative confocal images of mitochondria (green, TOMM20^{+}) and lysosomes (red, LAMP1^{+}) in K562 *WT*, or *SRSF2*$^{P95H/+}$ cells treated with DMSO or 3uM CHIR for 2d (left). Bar plot shows quantification of the co-localization of mitochondria with lysosomes (n=5 fields for each group. N=3). (C) Representative TEM images of *WT* and *SRSF2*$^{P95H/+}$ K562 cells treated with DMSO or 3μM CHIR for 2d (left). Bar plot (right) shows quantification of the number of autophagic vacuoles per cell. Each dot represents one cell. (D) Immunoblotting of PINK1 and β-catenin in *WT* and *SRSF2*$^{P95H/+}$ cells treated with DMSO or 3 uM CHIR for indicated times. (E) Violin plot of *OPTN*, *ULK1* and *TOMM7* normalized expression in AML patients in the TCGA dataset (n = 581) with or without mutations in *SRSF2*. Statistical analysis was performed using two-tailed Mann-Whitney test. (F) Overall survival (OS) of AML patients (n = 106) separated into two subgroups based on high and low expression of *OPTN* in publicly available TCGA datasets. Group cutoff for high and low expression was set to median (50%). Statistical analysis was performed using Mantel-Cox test.

Figure 6. The *SRSF2* mutation is associated with accumulation of defective mitochondria (A-B) Gene ontology enrichment analysis of differentially spliced genes in *SRSF2* mutant cells versus *WT* K562 cells (A) and primary CMML and AML patient samples (B). Bar graphs show significantly dysregulated pathways that are associated with mitochondrial functions, with Fisher's exact test -log[q-value] on X-axis. (C) Venn diagram showing overlap of proteins differentially expressed in *SRSF2*$^{P95H/+}$

versus *WT* K562 cells and MitoCarta 3.0 database. (D) Bar graph shows Log2 ratio of selected mitochondrial protein in *SRSF2*$^{P95H/+}$ vs. *SRSF2*$^{+/+}$ K562 cells. (E-G) Quantification of mitochondrial parameters in *WT* and *SRSF2*$^{P95H/+}$ cells (mean ± SD, n = 3). E, mitotracker green (MTG). F, Mitochondrial DNA copy number. Data are shown as ratio of mitochondrial DNA (mt-ND1) to nuclear DNA (B2M) in *wt* and *SRSF2*$^{P95H/+}$ cells. G, MMP per mitochondrion. (H) Basal, maximal, and complex I-linked mitochondrial respiratory capacity was measured in *WT* and *SRSF2*$^{P95H/+}$ cells. Maximal respiratory capacity was measured after FCCP injection. Complex I-linked respiration was measured by sequential addition of the complex I-linked substrates pyruvate, malate, and glutamate (P/M/G) and ADP. Oxygen flux expressed as respiration per million cells [pmol/(s·10^6 cells], mean ± SD of N = 3 independent cultures. Each sample was measured in duplicate. (I) Analysis of mitochondrial depolarization in *WT* and *SRSF2*$^{P95H/+}$ cells treated with DMSO or 2μM CCCP for 24h using JC-1 staining, in which a high Red$^+$:Green$^+$ ratio indicates high MMP (n=3). (J) Representive RT-PCR results of *PINK1* splicing in *WT* and *SRSF2*$^{P95H/+}$ cells treated with DMSO, 3μM CHIR or indicated concentrations of CCCP for 24h. (K) RT-qPCR analysis of *PINK1* mRNA levels in *WT* and *SRSF2*$^{P95H/+}$ cells treated with DMSO, 3μM CHIR, or 2μM CCCP for 24 h.

Figure 7. Targeting mitophagy in *SRSF2* mutant hematologic malignancies (A-B) Quantification of mitochondrial parameters in *WT* and *SRSF2*$^{P95H/+}$ cells treated with DMSO or 3μM CHIR (mean ± SD, n = 3). A, MMP per mitochondrion. B, MTG. (C) GSEA showing mitochondrial related enrichment plots for CHIR versus DMSO treated *WT* and *SRSF2*$^{P95H/+}$ cells. (D) Schematic of generating *WT* and *SRSF2*$^{P95H/+}$ stable lines overexpressing *PINK1* for apoptosis assay with or without CHIR. (E) Percentages of viable, early-, and late-apoptotic cells in *PINK1* overexpressing *WT* and *SRSF2*$^{P95H/+}$cells treated with DMSO or 3μM CHIR *in vitro* for 8d (mean ± SD, n=3). (F) Proposed model for dependency of *SRSF2* mutant leukemias on PINK1-mediated mitophagy and preferential cytotoxicity of GSK-3i and mitophagy inhibitor Chloroquine. (G) Quantification of mitochondrial mass by MTG staining in *WT* and *SRSF2*$^{P95H/+}$ cells treated with vehicle or indicated concentrations of Chloroquine for 6d (mean ± SD, n=3). (H) Percentage of viable cells based on 7-AAD and Annexin V flow cytometric analysis of *WT* and *SRSF2*$^{P95H/+}$ cells treated with vehicle or 20μM Chloroquine *in vitro* for 8d (mean ± SD, n=3). (I) Schematic representation of lentiviral delivery of *SRSF2*^{wt} or *SRSF2*^{P95H} to primary AML cells for Chloroquine treatment followed by apoptosis assay. (J) Representive flow cytometric analysis (left) and quantification (right) of apoptosis in primary cells from patient with AML overexpressing either *WT* or *SRSF2*^{P95H}, as measured by Annexin V and 7-AAD staining in absence or presence of 15μM Chloroquine for 4d.

Supplemental to Figure 1. (A) The *SRSF2*$^{P95H/+}$ mutation was analyzed by Sanger sequencing of genomic DNA (gDNA) isolated from isogenic K562 *WT* and *SRSF2*$^{P95H/+}$ cells (left). *WT* and *SRSF2*$^{P95H/+}$ cells were treated with increasing concentrations of CHIR for 3 days. Cell numbers were then determined by MTS absorbance. **: p<0.01. (B) *WT* and *SRSF2*$^{P95H/+}$ cells were cultured with vehicle or 10mM Lithium, and cell numbers were counted at day 2 and day 4 (mean ± SD). **: p<0.01. (C) Percentages of cells in G0, S/G2/M, and G1 based on Ki67 and DAPI cytometric analysis of isogenic K562 *WT*, *SRSF2*$^{P95H/+}$ and *SF3B1*$^{K700E/+}$ cells treated with DMSO or 3μM CHIR *in vitro* for 4 d (mean ± SD). (D-E) Validation of lentiviral infection efficacy by flow cytometric analysis of mCherry$^+$ in K562 cells (D) and immunoblotting of flag-tag in sorted mCherry$^+$ TF-1 cells (E). (F) Plotted are mCherry$^+$ percentages measured during 9 days in culture and normalized to day 0 (mean ± SD, n = 3).

(G) Percentage of early-apoptotic cells based on flow cytometric analysis of 7-AAD and Annexin V in *SRSF2*^{wt}- or *SRSF2*^{P95H}-expressing TF-1 cells treated with DMSO or 1μM CHIR in vitro for 6 days (mean ± SD, n = 3). (H-I) Representative images of tumor (H), and mouse body weight (I) after 13 days of treatment are shown in NSG mice subcutaneously implanted with K562 isogenic cells with or without *SRSF2*$^{P95H/+}$ mutation.

Supplemental to Figure 3. (A) Western blot analysis of β-catenin protein expression to validate GSK-3 inhibition by CHIR in K562 *WT*, *SRSF2*$^{P95H/+}$ and *SF3B1*$^{K700E/+}$ cells for RNA-seq. (B) Volcano plot analysis of all transcripts in CHIR versus DMSO treated *WT*, *SRSF2*$^{P95H/+}$ and *SF3B1*$^{K700E/+}$ K562 cells. Log2[FoldChange] was calculated for each transcript using normalized reads counts. (C) Venn diagram showing the numbers of overlapping differentially expressed genes between CHIR and DMSO treated *WT*, *SRSF2*$^{P95H/+}$ and *SF3B1*$^{K700E/+}$ K562 cells. (D) Heat map showing z-scored expression of *BCL2* family genes compared to mean expression for untreated parental cells. (E) Plotted are percentages of early-apoptotic cells of isogenic *WT*, *SRSF2*$^{P95H/+}$ and *SF3B1*$^{K700E/+}$ K562 cells treated with 3μM CHIR, or 40nM A1155463 and normalized to vehicle treated controls (mean ± SD). (F) *BCL-X* isoform specific qPCR analysis of DMSO or CHIR treated *WT*, *SRSF2*$^{P95H/+}$, and *SF3B1*$^{K700E/+}$ K562 cells. Percentage of exon exclusion was quantified by *BCL-XS* mRNA levels normalized to total mRNA. (G) Heat map of PSI values for overlapping alternatively spliced genes between CHIR and DMSO in *WT*, *SRSF2*$^{P95H/+}$ and *SF3B1*$^{K700E/+}$ K562 cells. (H) Sashimi plots of *KBTBD3* (left) and quantification of exon inclusion percentage (right) in *WT* and *SRSF2*$^{P95H/+}$ cells treated with DMSO or CHIR. *: $p<0.05$.

Supplemental to Figure 5. (A) Representive RT-PCR results of *PINK1* splicing in TF-1 cells expressing either *WT* or *P95H* mutant *SRSF2* treated with DMSO or 1μM CHIR for 24h. (B) Violin plot of *OPTN*, *ULK1* and *TOMM7* normalized expression in AML patients in the TCGA dataset (n = 405) with or without mutations in *SF3B1*. Statistical analysis was performed using two-tailed Mann-Whitney test.

Supplemental to Figure 6. (A) Heat map showing splicing events using the 2168 differentially spliced isoforms between *WT* and *SRSF2*$^{P95H/+}$ cells (FDR < 0.05, dPSI > 10%). (B) Representative confocal images of mitochondria (TOMM20^{+}) in WT and *SRSF2*$^{P95H/+}$ cells are shown. (C-E) Quantification of mitochondrial mass by MTG staining in K562 (C), TF-1 (D), and primary AML (E) cells overexpressing *WT* or mutant (mut) *SRSF2* (mean ± SD, n=3).

Supplemental to Figure 7. (A) Schematic of lentivirus infection in TF-1 cells for MTG staining and apoptosis assay. (B-C) Quantification of mitochondrial mass by MTG staining (B) and apoptosis (C) in TF-1 cells overexpressing *WT* or mutant (mut) *SRSF2* treated with DMSO or 1μM CHIR for 8d (mean ± SD, n=3). *: $p<0.05$. (D) Chloroquine dose-response curves of *WT* and *SRSF2*$^{P95H/+}$ cells.

Supplemental Tables

Supplemental table 1 Clinical and genetic characteristics of primary AML and CMML patient samples.
Supplemental table 2 Differentially expressed genes in CHIR versus DMSO treated WT, *SRSF2*$^{P95H/+}$ and *SF3B1*$^{K700E/+}$ K562 cells with a cutoff of padj < 0.05 and log2[fold change]l > 1.

Supplemental table 3 Alternative splicing genes in CHIR versus DMSO treated WT, *SRSF2*$^{P95H/+}$ and *SF3B1*$^{K700E/+}$ K562 cells with a cutoff of false discovery rate (FDR) < 0.05 and dPSI >10%.
Supplemental table 4 Differentially expressed mitochondrial proteins in *SRSF2*$^{P95H/+}$ versus *SRSF2*$^{+/+}$ K562 cells.

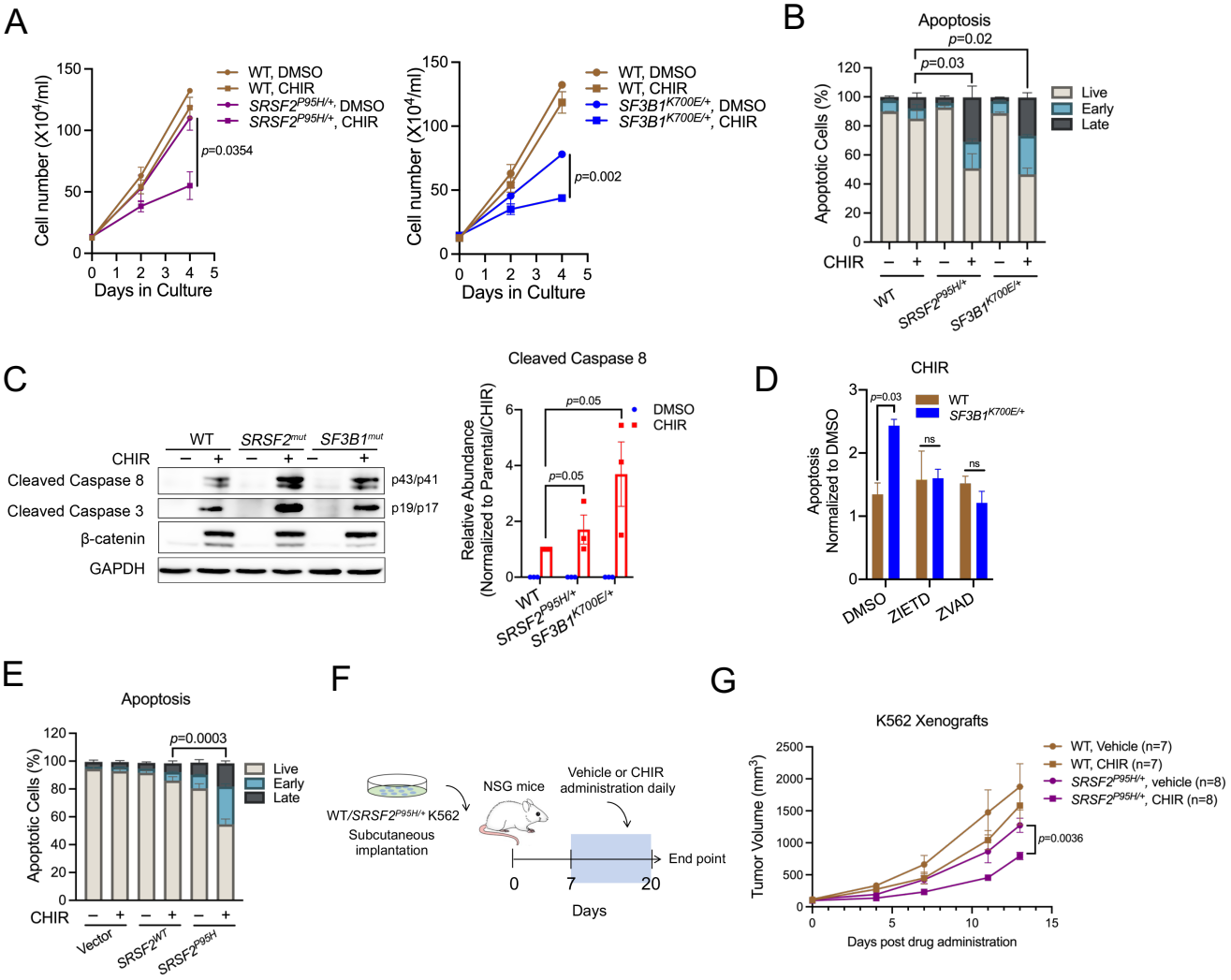
A
Cell number (X10^4/ml)
Days in Culture
WT, DMSO
WT, CHIR
SRSF2P95H/+, DMSO
SRSF2P95H/+, CHIR
p=0.0354
SF3B1K700E/+, DMSO
SF3B1K700E/+, CHIR
p=0.002
B
Apoptosis
p=0.02
p=0.03
Apoptotic Cells (%)
Live
Early
Late
CHIR
WT
SRSF2P95H/+
SF3B1K700E/+
C
WT
SRSF2mut
SF3B1mut
CHIR
Cleaved Caspase 8
Cleaved Caspase 3
β-catenin
GAPDH
p43/p41
p19/p17
Cleaved Caspase 8
Relative Abundance (Normalized to Parental/CHIR)
p=0.05
p=0.05
DMSO
CHIR
D
CHIR
Apoptosis Normalized to DMSO
p=0.03
ns
ns
DMSO
ZIETD
ZVAD
E
Apoptosis
p=0.0003
Apoptotic Cells (%)
Live
Early
Late
CHIR
Vector
SRSF2WT
SRSF2P95H
F
WT/SRSF2P95H/+ K562
Subcutaneous implantation
NSG mice
Vehicle or CHIR administration daily
End point
0
7
20
Days
G
K562 Xenografts
Tumor Volume (mm3)
Days post drug administration
WT, Vehicle (n=7)
WT, CHIR (n=7)
SRSF2P95H/+, vehicle (n=8)
SRSF2P95H/+, CHIR (n=8)
p=0.0036

Figure 1

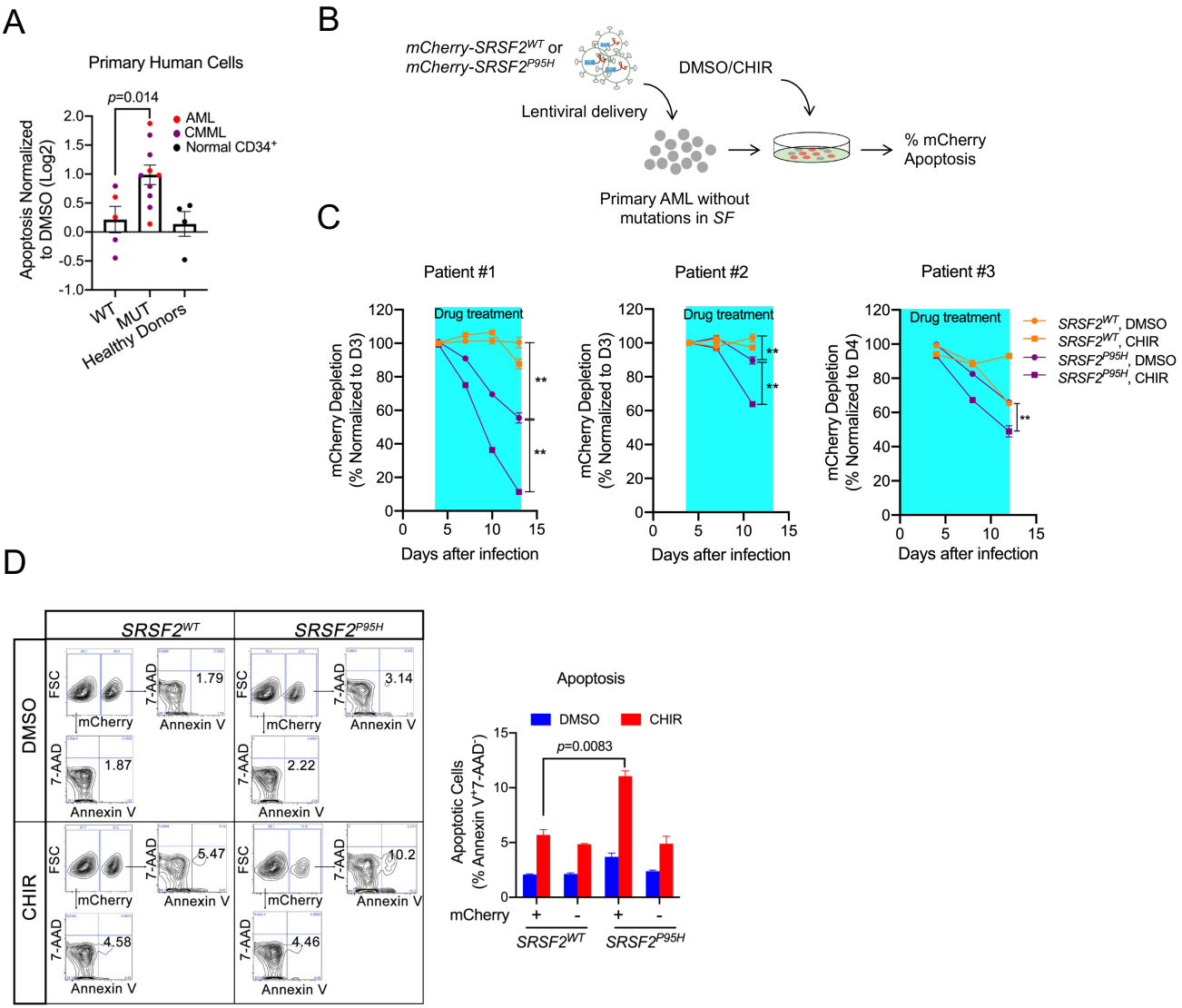
A
Primary Human Cells
p=0.014
AML
CMML
Normal CD34+
Apoptosis Normalized to DMSO (Log2)
WT
MUT
Healthy Donors
B
mCherry-SRSF2WT or mCherry-SRSF2P95H
DMSO/CHIR
Lentiviral delivery
% mCherry Apoptosis
Primary AML without mutations in SF
C
Patient #1
Patient #2
Patient #3
Drug treatment
mCherry Depletion (% Normalized to D3)
mCherry Depletion (% Normalized to D4)
Days after infection
SRSF2WT, DMSO
SRSF2WT, CHIR
SRSF2P95H, DMSO
SRSF2P95H, CHIR
D
SRSF2WT
SRSF2P95H
DMSO
CHIR
FSC
mCherry
7-AAD
Annexin V
1.79
3.14
1.87
2.22
5.47
10.2
4.58
4.46
Apoptosis
DMSO
CHIR
p=0.0083
Apoptotic Cells (% Annexin V+7-AAD-)
mCherry
+
-
+
-
SRSF2WT
SRSF2P95H

Figure 2

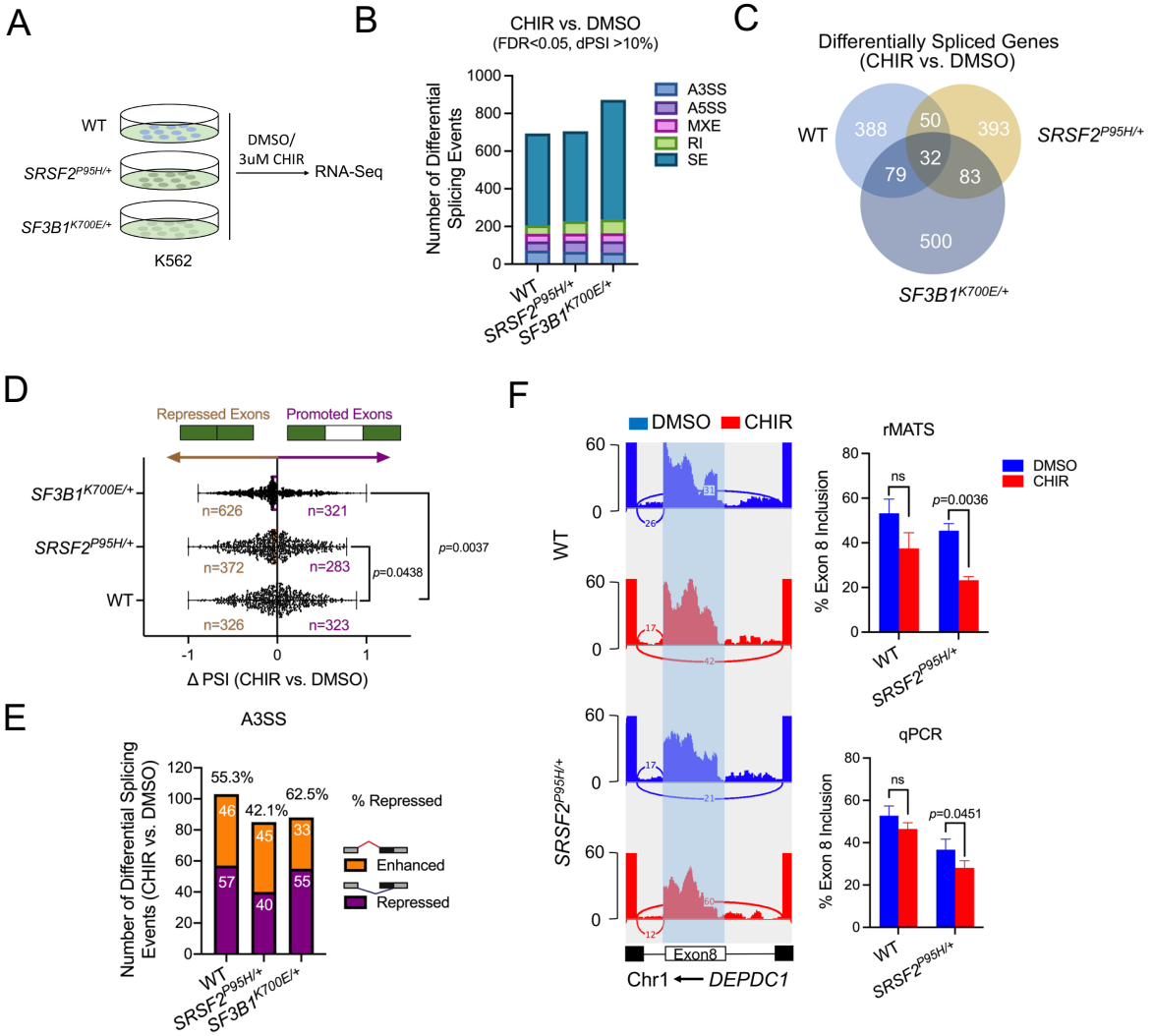
A
WT
SRSF2P95H/+
SF3B1K700E/+
K562
DMSO/
3uM CHIR
RNA-Seq
B
CHIR vs. DMSO
(FDR<0.05, dPSI >10%)
Number of Differential Splicing Events
A3SS
A5SS
MXE
RI
SE
C
Differentially Spliced Genes
(CHIR vs. DMSO)
388
50
393
32
79
83
500
D
Repressed Exons
Promoted Exons
n=626
n=321
n=372
n=283
n=326
n=323
p=0.0037
p=0.0438
Δ PSI (CHIR vs. DMSO)
E
A3SS
Number of Differential Splicing Events (CHIR vs. DMSO)
55.3%
42.1%
62.5%
% Repressed
Enhanced
Repressed
F
DMSO
CHIR
rMATS
% Exon 8 Inclusion
ns
p=0.0036
qPCR
p=0.0451
Exon8
Chr1 ⟵ DEPDC1

Figure 3

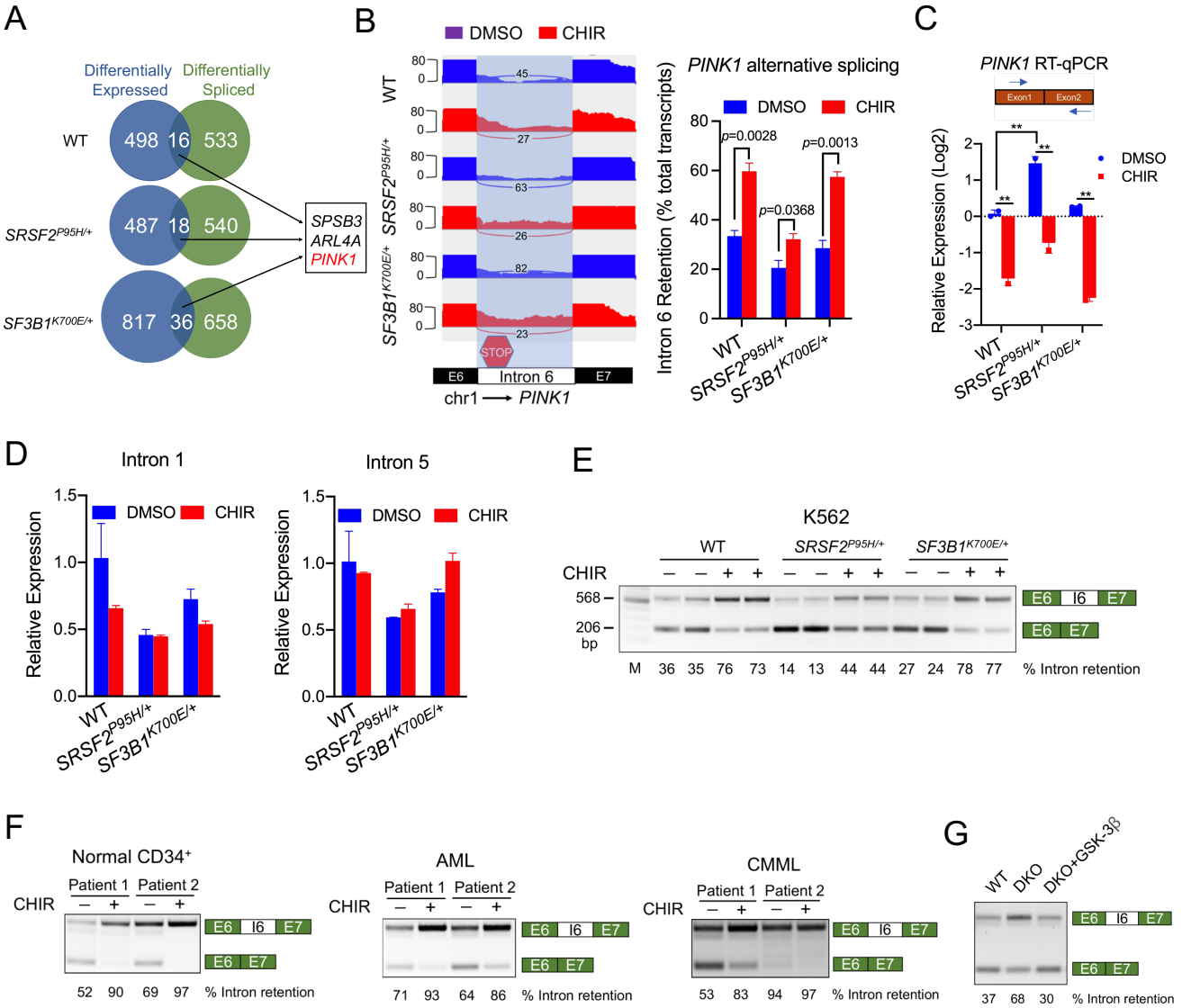
A
Differentially Expressed
Differentially Spliced
WT
498
16
533
SRSF2P95H/+
487
18
540
SF3B1K700E/+
817
36
658
SPSB3
ARL4A
PINK1
B
DMSO
CHIR
WT
SRSF2P95H/+
SF3B1K700E/+
45
27
63
26
82
23
STOP
E6
Intron 6
E7
chr1 → PINK1
PINK1 alternative splicing
Intron 6 Retention (% total transcripts)
p=0.0028
p=0.0368
p=0.0013
C
PINK1 RT-qPCR
Exon1
Exon2
Relative Expression (Log2)
D
Intron 1
Intron 5
Relative Expression
E
K562
CHIR
568
206
bp
M
36 35 76 73 14 13 44 44 27 24 78 77
% Intron retention
E6 I6 E7
E6 E7
F
Normal CD34+
AML
CMML
Patient 1
Patient 2
52 90 69 97
71 93 64 86
53 83 94 97
G
WT
DKO
DKO+GSK-3β
37 68 30

Figure 4

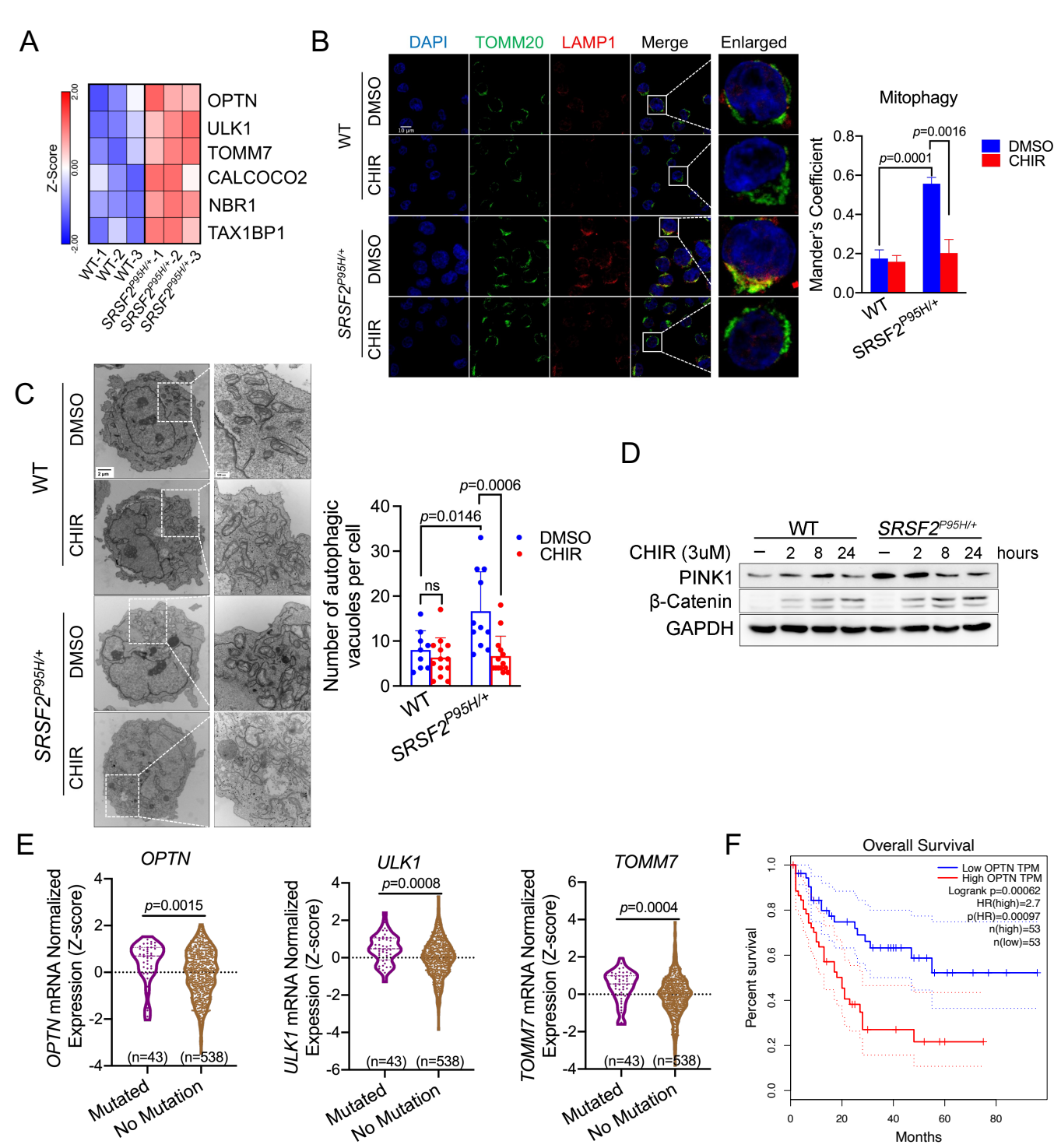
A
Z-Score
2.00
0.00
-2.00
OPTN
ULK1
TOMM7
CALCOCO2
NBR1
TAX1BP1
WT-1
WT-2
WT-3
SRSF2P95H/+-1
SRSF2P95H/+-2
SRSF2P95H/+-3
B
DAPI
TOMM20
LAMP1
Merge
Enlarged
WT
DMSO
CHIR
SRSF2P95H/+
DMSO
CHIR
Mitophagy
Mander's Coefficient
p=0.0016
p=0.0001
DMSO
CHIR
WT
SRSF2P95H/+
C
WT
DMSO
CHIR
SRSF2P95H/+
DMSO
CHIR
Number of autophagic vacuoles per cell
p=0.0006
p=0.0146
ns
DMSO
CHIR
WT
SRSF2P95H/+
D
WT
SRSF2P95H/+
CHIR (3uM)
–
2
8
24
–
2
8
24
hours
PINK1
β-Catenin
GAPDH
E
OPTN
OPTN mRNA Normalized Expression (Z-score)
p=0.0015
(n=43)
(n=538)
Mutated
No Mutation
ULK1
ULK1 mRNA Normalized Expression (Z-score)
p=0.0008
(n=43)
(n=538)
Mutated
No Mutation
TOMM7
TOMM7 mRNA Normalized Expression (Z-score)
p=0.0004
(n=43)
(n=538)
Mutated
No Mutation
F
Overall Survival
Low OPTN TPM
High OPTN TPM
Logrank p=0.00062
HR(high)=2.7
p(HR)=0.00097
n(high)=53
n(low)=53
Percent survival
Months

Figure 5

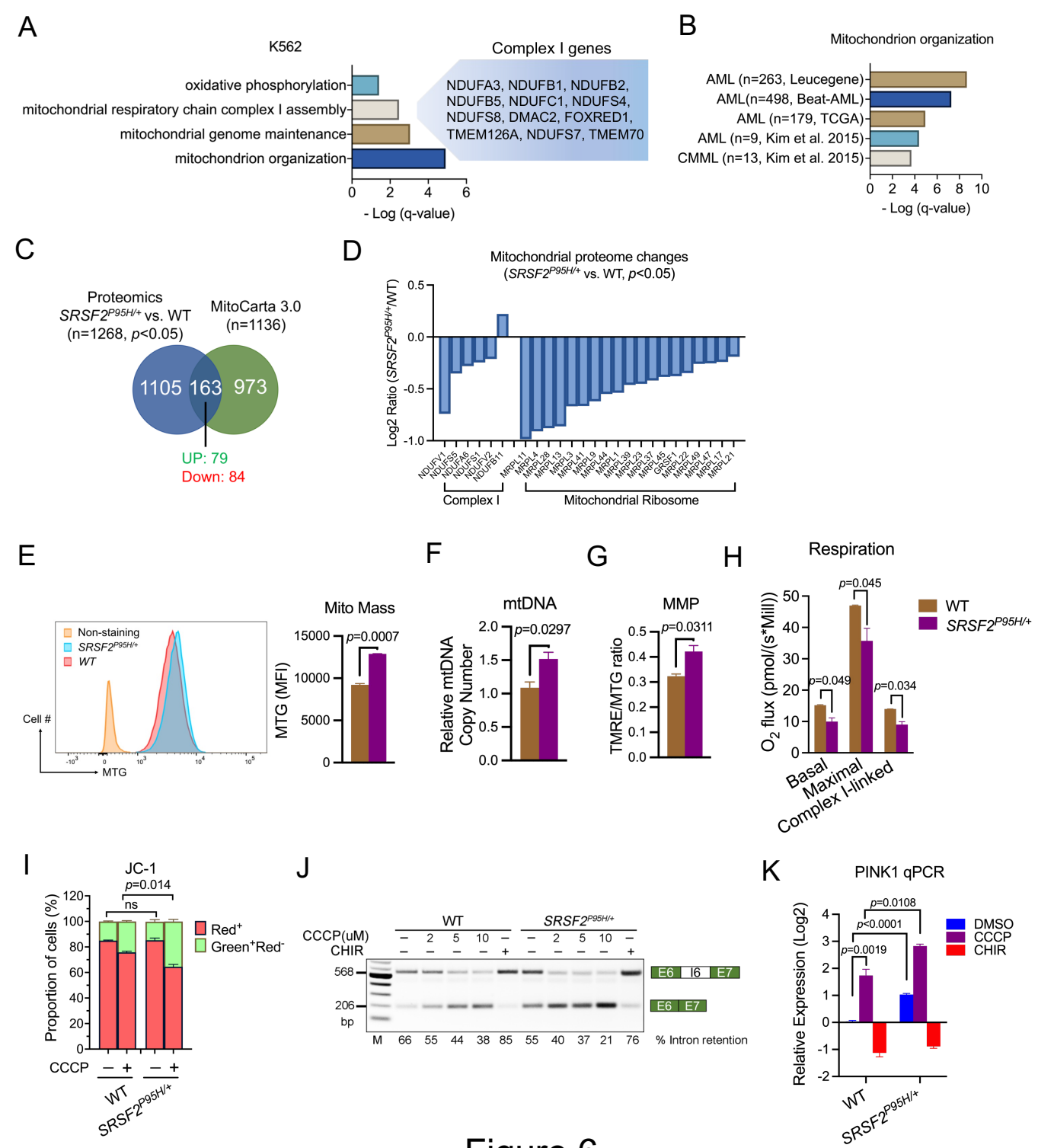
A
K562
Complex I genes
oxidative phosphorylation
mitochondrial respiratory chain complex I assembly
mitochondrial genome maintenance
mitochondrion organization
NDUFA3, NDUFB1, NDUFB2, NDUFB5, NDUFC1, NDUFS4, NDUFS8, DMAC2, FOXRED1, TMEM126A, NDUFS7, TMEM70
- Log (q-value)
B
Mitochondrion organization
AML (n=263, Leucegene)
AML(n=498, Beat-AML)
AML (n=179, TCGA)
AML (n=9, Kim et al. 2015)
CMML (n=13, Kim et al. 2015)
- Log (q-value)
C
Proteomics
SRSF2P95H/+ vs. WT
(n=1268, p<0.05)
MitoCarta 3.0
(n=1136)
1105
163
973
UP: 79
Down: 84
D
Mitochondrial proteome changes
(SRSF2P95H/+ vs. WT, p<0.05)
Log2 Ratio (SRSF2P95H/+/WT)
Complex I
Mitochondrial Ribosome
E
Non-staining
SRSF2P95H/+
WT
Cell #
MTG
Mito Mass
MTG (MFI)
p=0.0007
F
mtDNA
Relative mtDNA Copy Number
p=0.0297
G
MMP
TMRE/MTG ratio
p=0.0311
H
Respiration
O2 flux (pmol/(s*Mill))
WT
SRSF2P95H/+
p=0.045
p=0.049
p=0.034
Basal
Maximal
Complex I-linked
I
JC-1
p=0.014
ns
Proportion of cells (%)
Red+
Green+Red-
CCCP
WT
SRSF2P95H/+
J
WT
SRSF2P95H/+
CCCP(uM)
CHIR
568
206
bp
E6
I6
E7
M
% Intron retention
K
PINK1 qPCR
p=0.0108
p<0.0001
p=0.0019
DMSO
CCCP
CHIR
Relative Expression (Log2)
WT
SRSF2P95H/+

Figure 6

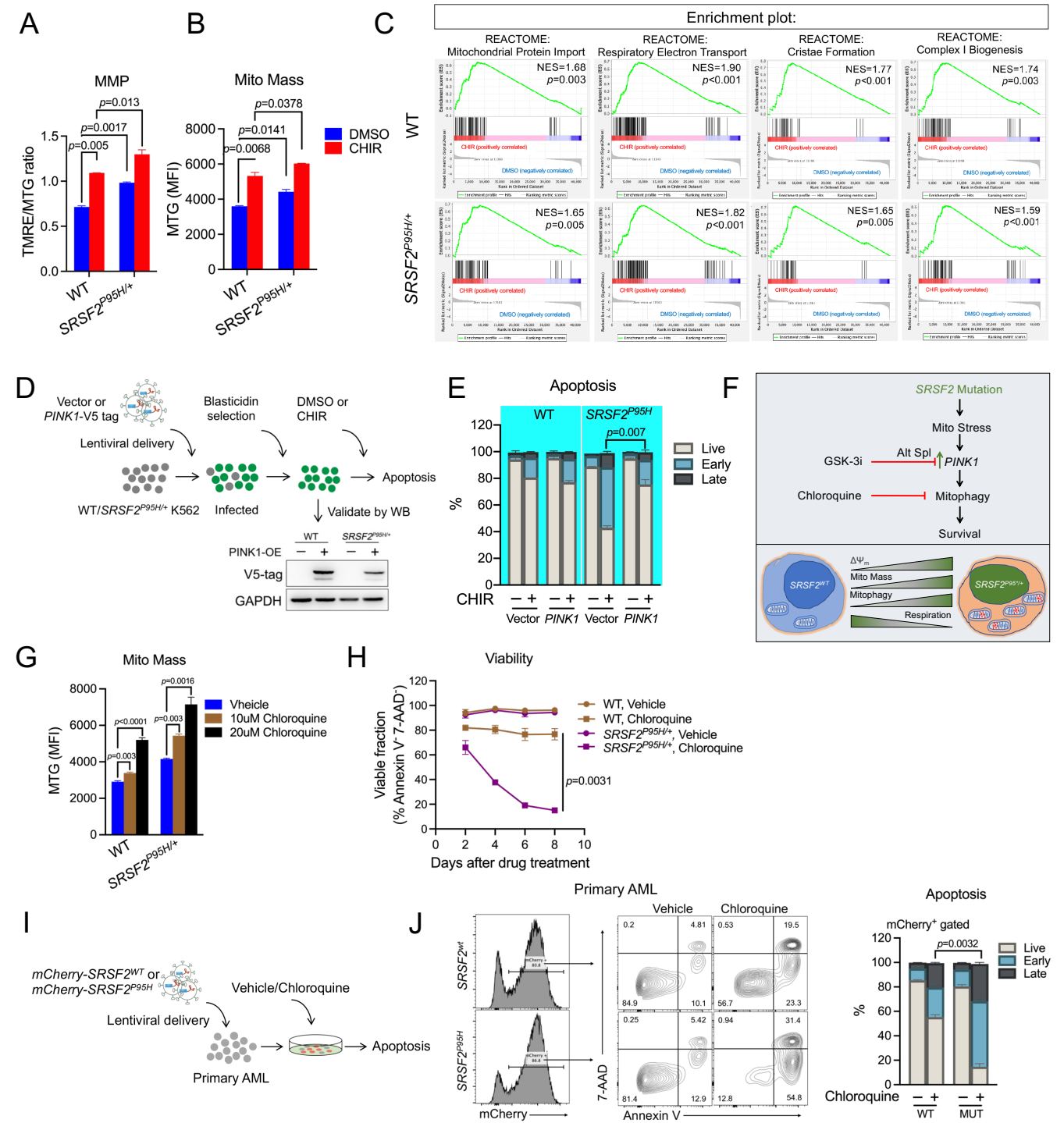
A
MMP
TMRE/MTG ratio
p=0.013
p=0.0017
p=0.005
WT
SRSF2P95H/+
B
Mito Mass
MTG (MFI)
p=0.0378
p=0.0141
p=0.0068
DMSO
CHIR
C
Enrichment plot:
REACTOME: Mitochondrial Protein Import
REACTOME: Respiratory Electron Transport
REACTOME: Cristae Formation
REACTOME: Complex I Biogenesis
NES=1.68 p=0.003
NES=1.90 p<0.001
NES=1.77 p<0.001
NES=1.74 p=0.003
NES=1.65 p=0.005
NES=1.82 p<0.001
NES=1.65 p=0.005
NES=1.59 p<0.001
CHIR (positively correlated)
DMSO (negatively correlated)
D
Vector or PINK1-V5 tag
Lentiviral delivery
Blasticidin selection
DMSO or CHIR
Apoptosis
WT/SRSF2P95H/+ K562
Infected
Validate by WB
PINK1-OE
V5-tag
GAPDH
E
Apoptosis
WT
SRSF2P95H
p=0.007
Live
Early
Late
CHIR
Vector
PINK1
F
SRSF2 Mutation
Mito Stress
GSK-3i
Alt Spl
PINK1
Chloroquine
Mitophagy
Survival
ΔΨm
Mito Mass
Mitophagy
Respiration
G
Mito Mass
MTG (MFI)
p<0.0001
p=0.003
p=0.003
p=0.0016
Vheicle
10uM Chloroquine
20uM Chloroquine
H
Viability
Viable fraction (% Annexin V-7-AAD-)
WT, Vehicle
WT, Chloroquine
SRSF2P95H/+, Vehicle
SRSF2P95H/+, Chloroquine
p=0.0031
Days after drug treatment
I
mCherry-SRSF2WT or mCherry-SRSF2P95H
Lentiviral delivery
Vehicle/Chloroquine
Apoptosis
Primary AML
J
Primary AML
Vehicle
Chloroquine
SRSF2wt
SRSF2P95H
mCherry
7-AAD
Annexin V
Apoptosis
mCherry+ gated
p=0.0032
Live
Early
Late
Chloroquine
WT
MUT

Figure 7

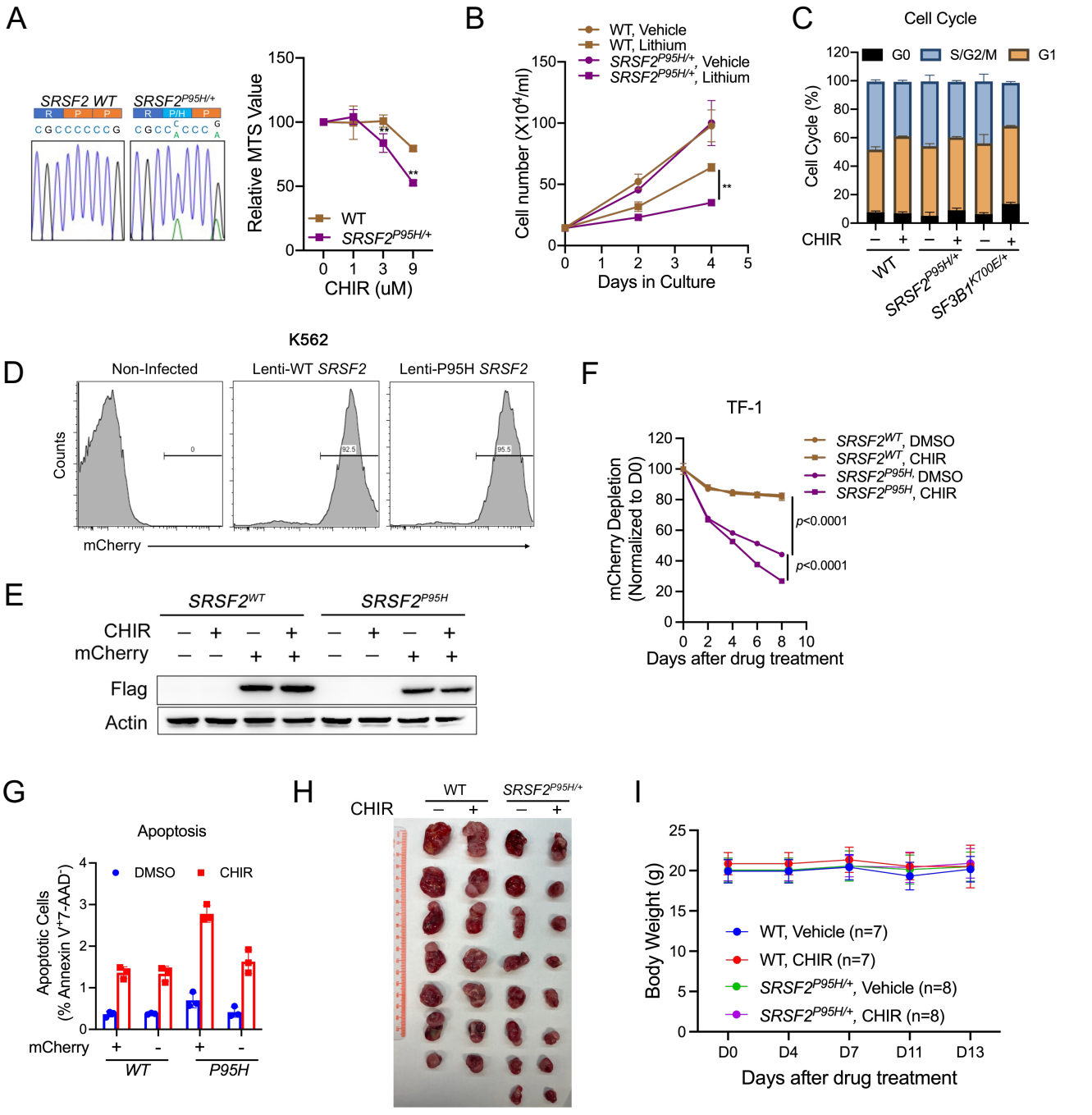

Supplemental to Figure 1

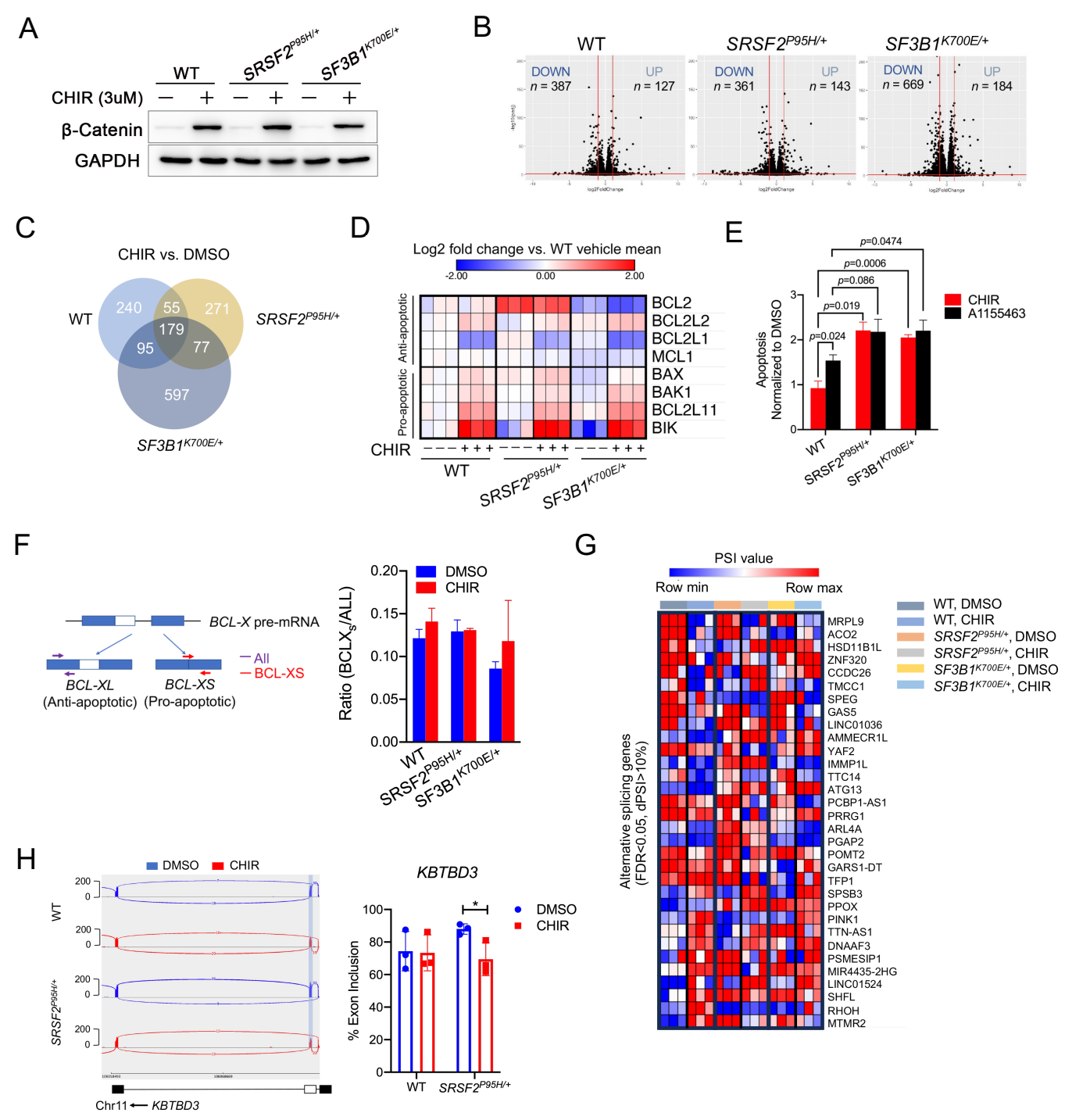

Supplemental to Figure 3

A

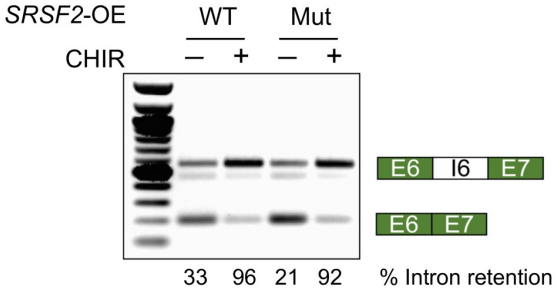

B

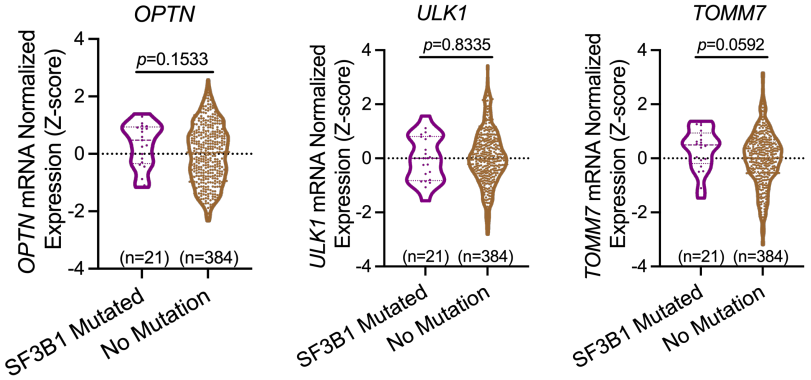

Supplemental to Figure 5

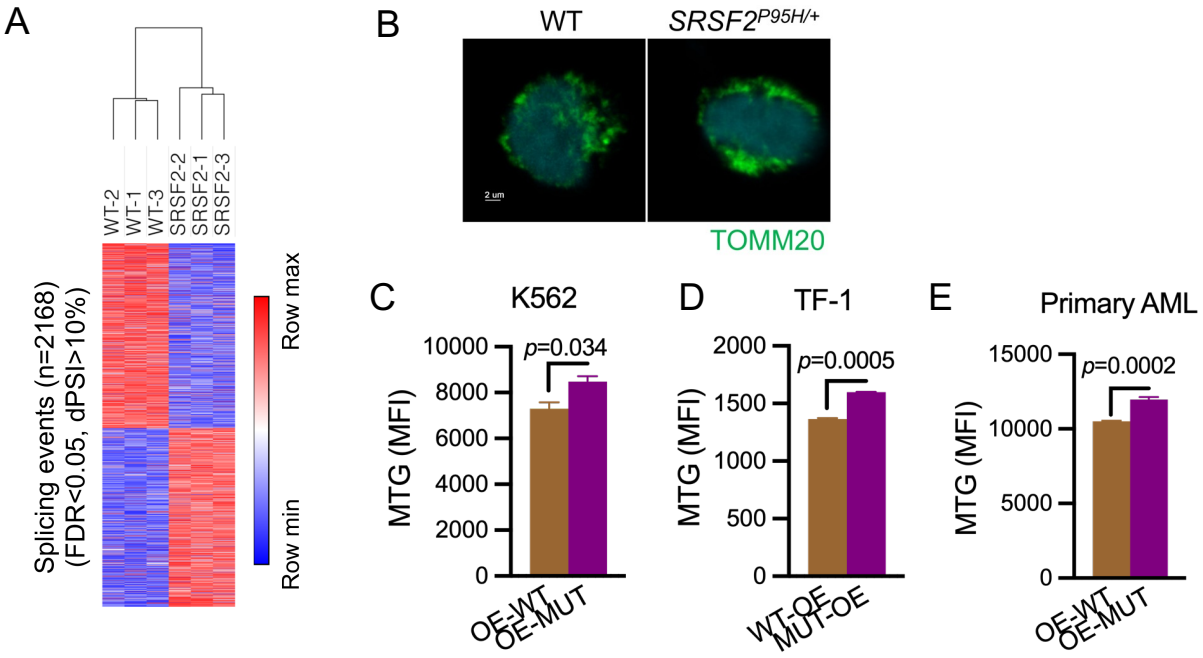

Supplemental to Figure 6

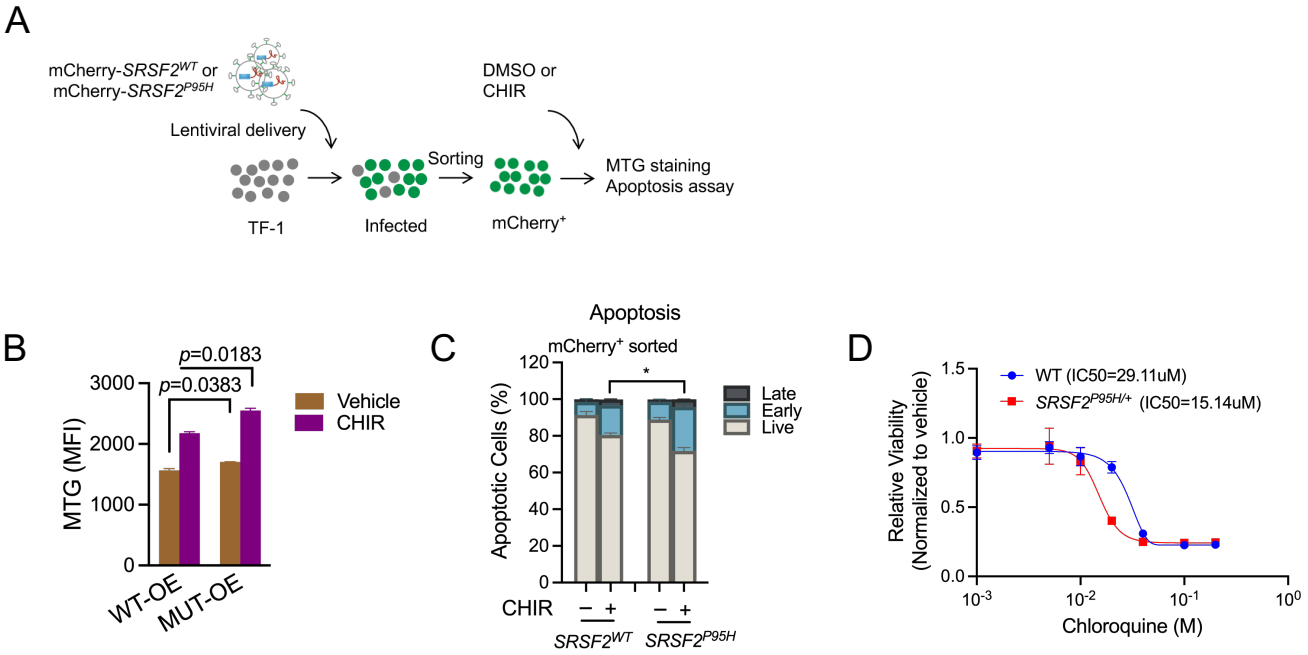

Supplemental to Figure 7